AD-A169 583 AIRCRAFT DRAG PREDICTION AND REDUCTION ADDENDUM 1(U) 1/1
ADVISORY GROUP FOR AEROSPACE RESEARCH AND DEVELOPMENT
NEUILLY-SUR-SEINE (FRANCE) J W SLOOFF APR 86
UNCLASSIFIED AGARD-R-723-ADD-1 F/G 20/4 NL

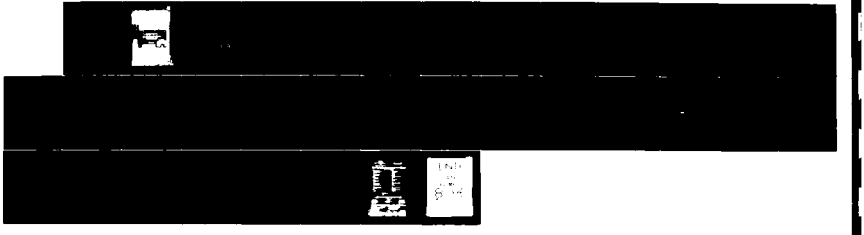

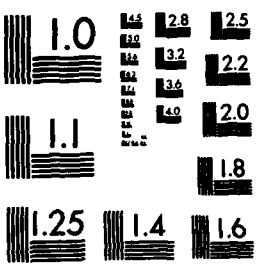

MICROCOPY RESOLUTION TEST CHART
NATIONAL BUREAU OF STANDARDS-1963-A

AD-A169 583

AGARD-R-723
Addendum 1

NORTH ATLANTIC TREATY ORGANIZATION

ADVISORY GROUP FOR AEROSPACE RESEARCH AND DEVELOPMENT

(ORGANISATION DU TRAITE DE L'ATLANTIQUE NORD)

AGARD Report No. 723

Addendum 1

AIRCRAFT DRAG PREDICTION AND REDUCTION

Computational Drag Analyses and Minimization; Mission Impossible?

by

J.W.Slooff
National Aerospace Laboratory (NLR)
Amsterdam, The Netherlands

DTIC
ELECTE
JUL 7 1986
S D
B

DISTRIBUTION STATEMENT A
Approved for public release;
Distribution Unlimited

The material assembled in this report was prepared under the combined sponsorship of the von Kármán Institute and the Fluid Dynamics Panel of AGARD and was presented as an AGARD Special Course at the von Kármán Institute, Rhode-Saint-Genèse, Belgium on 20—23 May 1985 and NASA Langley, USA on 5—8 August 1985.

THE MISSION OF AGARD

The mission of AGARD is to bring together the leading personalities of the NATO nations in the fields of science and technology relating to aerospace for the following purposes:

- Exchanging of scientific and technical information;
- Continuously stimulating advances in the aerospace sciences relevant to strengthening the common defence posture;
- Improving the co-operation among member nations in aerospace research and development;
- Providing scientific and technical advice and assistance to the Military Committee in the field of aerospace research and development (with particular regard to its military application);
- Rendering scientific and technical assistance, as requested, to other NATO bodies and to member nations in connection with research and development problems in the aerospace field;
- Providing assistance to member nations for the purpose of increasing their scientific and technical potential;
- Recommending effective ways for the member nations to use their research and development capabilities for the common benefit of the NATO community.

The highest authority within AGARD is the National Delegates Board consisting of officially appointed senior representatives from each member nation. The mission of AGARD is carried out through the Panels which are composed of experts appointed by the National Delegates, the Consultant and Exchange Programme and the Aerospace Applications Studies Programme. The results of AGARD work are reported to the member nations and the NATO Authorities through the AGARD series of publications of which this is one.

Participation in AGARD activities is by invitation only and is normally limited to citizens of the NATO nations.

The content of this publication has been reproduced
directly from material supplied by AGARD or the authors.

Published April 1986

Copyright © AGARD 1986
All Rights Reserved

ISBN 92-835-1524-2

Printed by Specialised Printing Services Limited
40 Chigwell Lane, Loughton, Essex IG10 3TZ

PREFACE

With diminishing world fuel supplies, and a global increase in fuel price over the last ten years, the reduction of aircraft drag has become a technology of major importance to aircraft manufacturers. Likewise, advances in test and evaluation techniques have facilitated the accurate evaluation of drag and led to concurrent developments in drag prediction methods. A noteworthy development is the use of a number of novel flow control methods which, through either passive or active interaction with the flow physics, can lead to substantial drag reductions.

This special course covers some of the more recent progress in drag reduction, measurement and prediction. The topics presented discuss the different sources and contributions to aircraft drag with particular emphasis on those areas in which significant new developments have taken place.

The course begins with a general review of drag reduction technology. Then the possibility of reduction of skin friction through control of laminar flow is discussed, with design aspects of laminar flow control hardware included. The other possibility of skin friction reduction through modification of the structure of the turbulence in the boundary layer is also discussed.

Methods for predicting and reducing the drag of external stores, of nacelles, of fuselage protuberances, and of fuselage afterbodies are then presented.

Transonic drag rise, the prediction of viscous and wave drag by a method matching inviscid flow calculations and boundary layer integral calculations, and the reduction of transonic drag through boundary layer control are also discussed.

QUALITY INSPECTED 1

Accession For
NTIS GRA&I
DTIC TAB
Unannounced
Justification
By
Distribution/
Availability Codes
Dist | Avail and/or Special
A-1

SPECIAL COURSE STAFF

Special Course Director: Dr A.S.W.Thomas
D72—74, Z 403
Lockheed Georgia Co.
86 South Cobb Drive
Marietta, GA 30063
United States

LECTURERS

Mr D.M.Bushnell
Head, Viscous Flow Branch
High-Speed Aerodynamics Division
NASA Langley Research Center
Hampton VA 23665
USA

Mr M.C.Fischer
ACEE Project Office
Mail Stop 158
NASA Langley Research Center
Hampton VA 23665
USA

Dr J.Hackett
D72—74, Z 403
Lockheed Georgia Co.
86 South Cobb Drive
Marietta, GA 30063
USA

Mr R.C.Lock
Aerodynamics Department
Royal Aircraft Establishment
Farnborough, Hants GU14 6TD
UK

M. Ph. Poisson-Quinton
ONERA
B.P. 72
92322 Châtillon
France

Dr W.S.Saric
Mechanical & Aerospace Engineering
Arizona State University
Tempe, AZ 85287
USA

Dr Ing. E.Stanewsky
DFVLR
Bunsenstrasse 10
3400 Göttingen
Federal Republic of Germany

Mr J.W.Slooff
NLR
Amsterdam
The Netherlands

LOCAL COORDINATOR

Professor M.Carbonaro
Von Kármán Institute for Fluid Dynamics
Chaussée de Waterloo 72
B-1640 Rhode-Saint-Genèse
Belgium

AGARD REPRESENTATIVE

Mr R.H.Rollins II
Fluid Dynamics Panel Executive
7 rue Ancelle
92200 Neuilly-sur-Seine
France

COMPUTATIONAL DRAG ANALYSES AND MINIMIZATION; MISSION IMPOSSIBLE?

by
J.W. Slooff
National Aerospace Laboratory (NLR)
Amsterdam, The Netherlands

SUMMARY

A discussion is given of the possibilities and problems associated with drag prediction, analysis and minimization by means of computational fluid dynamics (CFD) techniques based on inviscid and viscous-inviscid interaction flow models.
Attention is paid to
- classical and computational means of distinguishing between various drag components
- how to obtain values of drag components from currently available CFD codes and the problem of accuracy
- examples of computational drag diagnostics
- computational drag minimization

The discussion is limited, in essence, to sub/transonic transport (wing) aerodynamics, but should, at least partly, also be applicable to sub/transonic aerodynamics of fighter aircraft.

1 INTRODUCTION

The accurate prediction of aircraft aerodynamic drag is a generally recognized and respected problem. So is the accurate measurement of drag in the wind tunnel that, eventually, forms the basis for full scale drag prediction.

In the past 15 years Computational Fluid Dynamics (CFD) has emerged as an additional and complementary tool for aerodynamic design and analysis. The purpose of this lecture is to review and comment on its role as a drag prediction and analysis tool.

The aerodynamic design process of aircraft is characterized by a sequence of design and analysis cycles. In each cycle a (further) reduction of drag will, generally, be one, but not the only objective. Identification of the source of an unacceptably or undesirably high drag level or drag variation with lift or Mach number is a prerequisite for a successful drag reduction program.

Identification of drag sources may follow different approaches. The classical or phenomenological one is based on the availability of overall force (wind tunnel) data only, in combination with simple, semi-empirical theory. CFD, as we shall see later, offers possibilities for a more physically/analytically oriented approach in which the various contributions to drag are distinguished by the underlying physical mechanisms rather than by the observed aerodynamic force variation phenomena.

The main part of this lecture is directed towards the question of how the various components of drag, that can be distinguished, are modelled by, and can be obtained from the currently available CFD codes. As will be illustrated through examples, accuracy, in this context, is a crucial issue.

It will also be demonstrated that, in spite of its current shortcomings, CFD is a powerful tool for drag diagnostics. The final part of the lecture contains a discussion on computational drag minimization.

2 DRAG ANALYSIS, INTRODUCTORY REMARKS

There are various possible ways of distinguishing between different components of aerodynamic drag, e.g.
- according to the type of force acting on the body, i.e. pressure or friction drag (Fig. 1)
- according to the physical mechanisms that are responsible for drag, i.e. friction, causing "viscous" drag, vortex shedding, responsible for induced drag, and shock wave formation, causing wave drag (Fig. 2).

Viscous drag manifests itself partly as friction drag and partly as pressure drag. The other two as pressure drag only. Neither of the two classifications given above is fully manageable in a situation in which only total force data are available, such as in routine (balance) measurements in a wind tunnel. For this reason the classical approach to drag analyses is based on the observation of characteristic features in the variation of drag with, e.g., lift and Mach number. We may call this the phenomenological approach. In the phenomenological approach distinction is usually made between
- (subsonic) minimum drag; $C_{D_{min}}$
- (subsonic) drag-due-to-lift; C_{D_L}
- compressibility drag; $\Delta C_{D_{compr}}$
- trim drag; $\Delta C_{D_{trim}}$
- miscellaneous drag (due to excrescenses, etc); $\Delta C_{D_{misc}}$

In other words, the total drag is written as

$$C_{D_{tot}} = C_{D_{min}} + C_{D_L} + \Delta C_{D_{compr}} + \Delta C_{D_{trim}} + \Delta C_{D_{misc}} \qquad (1)$$

or a similar expression.
The (subsonic) minimum drag (Fig. 3) and drag-due-to-lift (Fig. 4) are usually defined at some suitable subcritical free stream Mach number such as M = 0.5 or 0.6. Compressibility drag is defined on the same basis (Fig. 5).

As defined above, $C_{D_{min}}$ contains most of the "viscous drag" and some induced drag. However, a distinc-

tion between the two can usually not be made unless detailed knowledge about the span loading of the wing is available. In preliminary design studies $C_{D_{min}}$ is usually estimated by means of the classical "form factor" methods that, e.g. can be found in Hoerner's Book "Fluid Dynamic Drag", USAF DATCOM and the ESDU data sheets.

The (subsonic) drag due to lift contains most if not all of the induced drag, some viscous drag and, possibly, some wave drag at the higher lift values. It is usually estimated or fitted by means of the classical induced drag formula

$$C_{D_L} = \frac{[C_L - C_L(C_{D_{min}})]^2}{\pi Ae} \qquad (2)$$

the "Oswald" factor "e" accounting for the deviation of the spanwise load distribution from the elliptical one and for the variation of the viscous drag with lift.

Compressibility drag (Fig. 5) contains most if not all of the wave drag, the increase of viscous drag with Mach number and possibly some induced drag due to changes in span loading with Mach number. A general theoretical basis (apart from CFD means) for the prediction of wave drag does not exist.

Trim drag contains the induced drag increment of wing plus tail due to tail load plus some viscous drag and wave drag. The latter two because the wing, at least for conventional configurations, has to operate at a higher lift coefficient than untrimmed due to the negative tail load.

The classical or phenomenological approach, as mentioned, leads to a manageable way of distinguishing between drag components in case only overall force data are available. A disadvantage is, however, that it often remains difficult, if not impossible, to point-out the precise source of an undesirable drag "surprise". The reason being that these classically distinguished drag components do not reflect one single but, in fact, several physical mechanisms. In this respect an analytical approach to drag analysis, that distinguishes between the three major physical mechanisms, i.e. friction (viscosity), vortex shedding and shock wave formation, has certain advantages. As we shall see, CFD methods may serve such purpose.

3 CLASSIFICATION OF CFD METHODS WITH RESPECT TO DRAG PREDICTION POTENTIAL

Prior to going into the details of the possibilities and limitations of computational drag determination it is useful to summarize briefly which drag phenomena are modelled by the mathematical/physical models underlying the currently available CFD codes. Figs. 6 and 7 may serve this purpose.

Figure 6 presents the hierarchy of mathematical/physical flow models of interest for applied CFD purposes. Reynolds averaged Navier-Stokes methods can provide both friction drag and pressure drag and, at least in principle, contain all information to distinguish between viscous drag, induced drag and wave drag. However, because of the very large computational effort required, such methods are not (yet) generally available in the applied computational environment, at least for problems involving three dimensions. For this reason we will not pay any further attention to Navier-Stokes methods in this lecture note.

On the next level (zonal modelling) we must distinguish between inviscid flow and viscous flow (boundary layer) methods. The mutual interaction between the inviscid and viscous parts of the flow field is modelled through an interaction law describing the coupling between the two zones at a suitably chosen boundary.

The boundary layer methods model viscous drag only, subject to the boundary conditions provided by the external inviscid flow through the interaction law.

Three further levels of modelling with decreasing physical significance can be distinguished for inviscid flow. Methods based on the Euler equations model both induced drag and wave drag. So do methods based on the full potential equation for compressible flow, but as far as wave drag is concerned, in an approximate sense only. The approximation involved implies a limitation to weak or at most moderately strong shocks with a maximum normal Mach number of about 1.3. This, however, is acceptable for many practical purposes. Figure 8, taken from ref. 1, provides an impression of the accuracy of the potential flow model in relation to the Euler model for a shock Mach number of about 1.3.

Linear potential flow methods, such as panel methods, model induced drag only (plus a part of the wave drag in case of linearized supersonic flow).

4 DETERMINATION OF DRAG FROM CFD CODES

Generally speaking there are two different ways of obtaining drag values from CFD code application. One is the direct integration of pressure and friction forces. We will call this the near-field approach. The other is based on application of the momentum theorem to a control volume enclosing the configuration. We will call this the far-field approach.

4.1 "Near-field" assessment; pressure and friction drag

The accurate determination of pressure drag from wind tunnel pressure measurements is a well respected problem. The following examples illustrate that the problem is of comparable magnitude in CFD; at least in three dimensions, and if one does not have access to a sufficiently fast computer with sufficiently large memory.

Figure 9 presents an example of the pressure drag dependence on mesh density for a 2D lifting airfoil with a strong shock wave as calculated with a "state of the art" Euler code employing an O-type mesh (N being the number of mesh points). The results indicate that, for the particular case considered, a 196 x 36 mesh suffices to obtain a pressure drag coefficient value accurate to 1 "count" (10^{-4}). (The latter value seems to be widely accepted as a "target" accuracy for drag measurement in wind-tunnel testing). Similar results for a shock-free supercritical airfoil as obtained with two different Euler codes (of which one with several different distribution of mesh points) and a full potential code are presented in figure 10. All these codes use O-type meshes but with different distributions of mesh points.

The message of figure 10 is that the sensitivity of the results for mesh density depends strongly on the distribution of mesh points. For Euler code 1 this sensitivity is clearly unacceptably high for the

particular type of mesh used. For Euler code 2 it is seen to vary strongly with the distribution of mesh points. For the full potential code a 192x96 mesh is required for a 1 count accuracy.

It can be concluded from figures 9 and 10 that, with a suitable distribution of mesh points, a 200x50 to 200x100 mesh will generally be sufficient to obtain pressure drag values for 2D airfoils that are, numerically, accurate to 1 count. For the currently available general purpose type of main frame computer this is certainly feasible.

An aspect that may also affect the accuracy of CFD pressure drag prediction is mesh extent. The point is illustrated by figure 11 *). Shown is the depence of the pressure drag, as computed with a finite volume type Euler code, on the distance from the airfoil at which the far field boundary condition (in this case free stream plus asymptotic far-field vortex term) is prescribed. The particular case requires a mesh extent of about 100 chords for a 1 count accuracy! (This value would be reduced if a more accurate asymptotic far field boundary condition is used).

A 3D example of pressure drag dependence on mesh density is presented in figure 12. The case considered is an application of a modified FL022 code (Ref. 3) to a transport type wing with transonic flow. About 400 relaxation iterations were performed on each fine mesh plus successive mesh refinement. The figure illustrates that, for the particular C-type mesh utilized in these calculations, something of the order of 540 k mesh points are required for a (numerical) accuracy of 1 count if the calculations are performed for a given lift. The situation is distressingly worse if the calculations are performed for a given angle of attack.

Examples such as that of figure 12 serve to illustrate the point that the accurate determination of inviscid pressure drag for 3D wings is currently (almost) impossible in an engineering environment. The general experience is that this applies to finite difference/finite volume type field methods as well as "panel" methods. However, as we shall see later, this does not necessarily mean, that CFD, even now, cannot play a useful role in drag prediction/analyses studies.

The problem of the accurate prediction of the friction drag by means of boundary layer codes is of a somewhat different nature. Unlike the (current) situation with inviscid flow methods, numerical accuracy (truncation errors) is not the major source of concern in boundary layer calculations, the computational requirements being relatively modest. In boundary layer computations the "absolute" accuracy associated with the particular choice of mathematical/physical model is of greater importance. The most important factors involved are:

- type of method ("integral" of "field" method)
- transition and turbulence models
- type of interaction law used ("weak" or "strong")
- type of flow (attached or separated)

Examples of skin friction prediction, for low speed flows, are presented in figures 13, 14. In one case (Eppler airfoil) the agreement between measured and calculated skin-friction distribution is seen to be quite good. In the other case (upper surface of the main airfoil of a high-lift configuration) there is substantial disagreement between theory (4 different methods) and experiment, the reason of which is not clear. These examples illustrate that the accurate prediction of skin friction may not (yet) be taken for granted.

It is the author's general impression that the "absolute" errors involved in friction drag prediction may be as large as 5 to 15 counts for attached flows and possibly larger for separated flows. This, however, does not exclude the possibility to obtain meaningful predictions of friction drag for similar types of flow on similar configuration on an increment/decrement basis.

4.2 "Far-field assessment (momentum theorem)

Expressions for the drag acting on a body can also be derived by applying the momentum theorem to a control volume enclosing the body. In the following we will do so first for the case of purely inviscid flow and subsequently for inviscid flows with "viscous" interactions and boundary layer/wake flows ("zonal modelling").

4.2.1 Inviscid flow, general expressions

Consider a control volume of the type as indicated (for a half wing) in figure 15. In the far-field (S_∞) the volume is bounded by a plane normal to the x-axis far upstream of the wing, a similar plane (far) downstream and planes parallel to the x-z and x-y planes, respectively, each at a large distance from the wing. In the near-field the volume is bounded by the body (wing) surface (S_B) and (both sides of) the shock-wave (S_{shock}) and vortex sheet (S_{wake}) surfaces. The reasons for excluding the vortex sheet from the control volume is in the fact that the latter must be bounded by a single closed surface. Hence a cut must be introduced between S_B and $S_{(\infty)}$. The vortex sheet is a natural, and, as we shall see later, sometimes necessary choice for such a cut. The reason for excluding the shock surface will become apparent shortly.

Application of the conservation law for momentum to the control volume of figure 15 leads to the integral expression

$$\oint_S [p\, n_x + (\rho \bar{q}.\bar{n})u]\, dS = 0 \qquad (3)$$

where

$$S = S_B + S_{shock} + S_{wake} + S_{(\infty)}$$

p is the (local) static pressure, $\bar{q}$ is the total velocity vector, ρ is the density, $\bar{n}$ is the unit outward normal to the control volume (hence pointing inside S_B, S_{shock} and S_{wake}) and u is the component in the free-stream (x-) direction of $\bar{q}$.

*) Figs. 9, 10 and 11 have been derived from data contained by reference 2.

Splitting-off the body pressure integral from eq. (3) leads to the following relation for the pressure drag

$$D_p = \oiint_{S_B} p\, n_x\, dS =$$

$$= - \iint_{S+S_B} [p\, n_x + (\rho\, \bar{q}.\bar{n})\, u]\, dS - \oiint_{S_B} (\rho\, \bar{q}.\bar{n})\, u\, dS$$

This can be rearranged to read

$$D = - \underbrace{\iint_{S_{shock}} \left[p\, n_{1_x} + (\rho\, \bar{q}.\bar{n}_1)\, u\right]_2^1 dS}_{(I_1)} +$$

$$- \underbrace{\iint_{S_{wake}} \left[p\, n_{1_x} + (\rho\, \bar{q}.\bar{n}_1)\, u\right]_2^1 dS}_{(I_2)} +$$

$$- \underbrace{\iint_{S_{(\infty)}} [p\, n_x + (\rho\, \bar{q}.\bar{n})\, u]\, dS}_{(I_3)} +$$

$$- \underbrace{\iint_{S_B} (\rho\, \bar{q}.\bar{n})\, u\, dS}_{(I_4)} \qquad (5)$$

Here $[\quad]_2^1$ denotes a jump of the particular quantity across the particular surface of discontinuity. Note that, in the case of zero normal mass flux on the body and vortex sheet, which we will consider first, both I_4 and the second part of I_2 are zero. Note also that eq. (5) is equally valid in "full potential" flow and "Euler" flow. However, the various terms distinguished in eq. (5) have different meanings in these two flow models.

In the (time-dependent) Euler codes that are currently available, momentum, as well as mass and energy, are conserved in the whole of the flow field, including shocks and vortex sheets. The latter two are captured as narrow regions with high velocity gradient rather than discontinuities as a result of the numerical and artificial dissipation associated with the discretization schemes that are being used. Within these layers momentum is conserved to the (numerical) accuracy implied by these schemes. It follows that in the Euler flow model the integrals I_1 and I_2 of eq. (5), assuming vanishing truncation errors, are identical to zero. As already mentioned, the fourth integral (I_4) is also zero in case of zero normal velocity on S_B. Hence, the remaining term I_3, i.e. in the far-field integral, contains both the wave drag and the induced drag.

In (conservative) potential flow models mass as well as energy (and entropy) are conserved across shock waves, (or rather the shock layers that result from the numerical schemes), but momentum normal to the shock is not. The latter, in fact, is the very mechanism for the production of wave drag in potential flow models, as described by Steger and Baldwin, Ref. 6 (see also Van der Vooren and Slooff, Ref. 7). It also constitutes the reason for excluding the shock surface from the momentum control volume. In spite of the non-physical nature of this seemingly strange mechanism, potential flow methods generate useful numbers of "wave drag" as long as the component of the local Mach number normal to the shock does not exceed a value of say, 1.3. The point was already illustrated by figure 8.

From the discussion just given it follows, that in the potential flow model, the integral I_1 in eq. (5) is different from zero and represents (an approximation to) the wave drag. The far-field integral I_3 now contains the induced drag only. The integral I_4, as mentioned, is zero in case of zero normal mass flux on S_B. Remains to discuss the "wake" integral I_2 for the potential flow case.

In the currently available potential flow codes it is general practice to model the vortex sheet as a (curved) plane of discontinuity, coinciding with a plane of the computational mesh, that carries a jump in potential. The jump in potential is taken to be constant along the mesh lines in this plane which coincide, approximately, with the free stream direction. In addition the difference formulae utilized on both sides of this "vortex sheet" are chosen such that there is continuity of normal mass flux across the "vortex sheet". An implication of this is, that the "flux" term of momentum is continuous across the vortex sheet discontinuity but the pressure is continuous in a small perturbation sense only. Hence the term I_2 in eq. (5), although small, is not necessarily identical to zero in potential flow calculations with a priori selected fixed position of the vortex sheet. The author is not aware of any numerical assessment of this term, which, indeed, is generally neglected.

4.2.2 The evaluation of wave drag and induced drag from potential flow codes

In the preceeding paragraph we have seen that, in potential flow, the wave drag can be determined, at least in principle, by integrating the jump in momentum across the shoc surface(s), (term I_1 of eq. (5)). In practice it appears that the accurate determination of the wave drag along these lines poses several difficulties.

First of all, as noted before, shocks are smeared by numerical capturing schemes. This problem can be overcome by enlarging the contour of integration to ensure that the shock is completely enveloped and calculating the loss of momentum within this contour. Figure 16 shows permissible contours of integration.

The major problem associated with calculating the wave drag along these lines is the accurate numerical evaluation of the integral. It has been found (Yu, et.al., Ref. 8) that very fine meshes are required to perform the integration with acceptable accuracy and that the relaxation process for solving the flow equations must be continued to iteration levels that are far beyond those of current engineering practice. The reason for the latter is in the fact that any mass flux residual (source of sink like) acts as a spurious drag of thrust source. This must either be avoided by a large number of iterations or be corrected for, see reference 8.
Making use of the mass conservation law applied to the contour S_{shock} (Fig. 16)*), i.e.

$$- \iint_{S_{shock}} \rho \, \bar{q}.\bar{n} \, d S = R_{shock} \tag{6}$$

where R_{shock} represents the sum of the residual sources in the flow field within S_{shock}, the integral I_1 of eq. (5) can be written as

$$I_1 = - \iint_{S_{shock}} [p \, n_x + (u-u_\infty) \, \rho \, \bar{q}.\bar{n}] \, d S + u_\infty \, R_{shock} \tag{7}$$

With the second term of (7) representing the drag or thrust associated with any residual sources within S_{shock}, the first term represents the wave drag. I.e.:

$$D_{wave} = - \iint_{S_{shock}} [p \, n_x + (u-u_\infty) \, \rho \, \bar{q}.\bar{n}] \, d S = I_1' \tag{8}$$

The problem of accuracy is illustrated by figure 17 which was taken from reference 8. For a transport type of wing-body configuration with a mesh which is typical for current engineering practice, the calculated wave drag varies between 34 and 59 drag counts, depending on the integration contour selected. Evidently much finer grids (possibly of the order of (.5 to 1) x 10^6 gridpoints) are required to calculate the wave drag in this way with acceptable accuracy.
An interesting alternative way of evaluating the wave drag from potential flow codes has been proposed by Garabedian et.al., Ref. 9. They have shown that the integration of the artificial viscosity term over the supersonic part of the flow field provides a measure of the wave drag.

As discussed in section 4.2.1 the <u>induced drag</u> in potential flow is represented by the term I_3 of eq. (5). In analogy with the shock integral I_1, the term I_3 can be rewritten as

$$I_3 = - \iint_{S_{(\infty)}} [p \, n_x + (u-u_\infty) \, \rho \, \bar{q}.\bar{n}] \, d S + u_\infty \, [\iint_{S_B+S_{wake}} \rho \, \bar{q}.\bar{n} \, d S - R_{(\infty)}] \tag{9}$$

with $R_{(\infty)}$ defined by

$$\iint_{S_{(\infty)}} (\rho \, \bar{q}.\bar{n}) \, d S + \iint_{S_B+S_{wake}} \rho \, \bar{q}.\bar{n} \, d S = R_{(\infty)} \tag{10}$$

With the second term of eq. (9) again representing the drag acting on intentional and/or spurious sources, (within $S_{(\infty)}$), the induced drag is given by

$$D_i = - \iint_{S_{(\infty)}} [p \, n_x + (u-u_\infty) \, \rho \, \bar{q}.\bar{n}] \, d S = I_3' \tag{11}$$

In finite volume type of potential flow codes this integral can be evaluated on suitably chosen grid boundary planes. The experience appears to be (Ref. 8) that this can be done with acceptable numerical accuracy.
An alternative is to let the boundary surface $S_{(\infty)}$ of eq. (11) go to infinity in which case the integral reduces to the "Trefftz-plane" ($x=+\infty$) integral:

$$D_i = - \iint_{x=+\infty} [(p-p_\infty) + (u-u_\infty) \, \rho u] \, d S \tag{12}$$

Assuming small perturbations in the "Trefftz-plane", eq. (12) may be further simplified to the classical result (see figure 18)

$$D_i = \int_{S_{wake} \cap x=\infty} [\phi] \, .\bar{q}.\bar{n}_{wake} \, d t \tag{13}$$

For details of the derivation and approximations involved see e.g. Lock, Ref. 10. Note that eq. (13) can be used to calculate the drag from finite difference/finite volume type of calculations as well as from linear, panel type methods.
While the small perturbation assumptions on which eq. (13) is based are violated for high lift and low aspect ratio, and possibly at the (tip) edge of the vortex sheet in any case, the general experience (including the author's) is, that it leads to induced drag values of acceptable accuracy in many if not most practical cases.

---

*) Note the positive direction of the normals on S_{shock} and S_B!

4.2.3 The evaluation of drag from Euler codes

As discussed in section 4.2.1 the integral I_3 of eq. (5), or eq. (9), contains both the wave drag and the induced drag in "Euler flow", (as well as the drag associated with any spurious or real mass sources inside the flow field). Reportedly (Ref. 8), the numerical evaluation of the far field integral in Euler codes can be performed with acceptable accuracy in 2D, but not in 3D. The main problems seem to be inappropriate (far-field) boundary conditions, at least for this purpose, and lack of resolution due to the relatively small number of mesh points that can be afforded in engineering applications.

Splitting the total inviscid drag from the far-field integral into wave drag and induced drag parts is not a trivial matter. As discussed by Lock (Ref. 10) it can be done only under certain simplifying assumptions. To the author's knowledge it has not (yet) been attempted in actual 3D Euler applications. In the latter the problem is further exhanced by the fact that vortex sheets are captured as shear layers rather than discontinuities. Further exploration of the possibilities along these lines deserves attention.

A separate evaluation of the wave drag is possible by considering the entropy production of shock waves, or, rather, the entropy produced within a contour enveloping the numerically smeared shock layers (Fig. 19).
For this purpose use can be made of an expression originally derived by Oswatitsch (Ref. 11)

$$D_{wave} = \frac{T_\infty}{q_\infty} \int_{S_{shock}} (\tilde{S}-\tilde{S}_\infty)\, \rho\, \bar{q}.\bar{n}\, d\, s \qquad (14)$$

($\tilde{S}$ denoting entropy and T_∞ the freestream temperature), or variants thereof (see also Ref. 10).

The experience appears to be (Ref. 8) that eq. (14) can be evaluated with acceptable accuracy in 2D but not (yet) in 3D. The main problems being spurious entropy production (dissipation) associated with the numerical schemes, in particular near the flow boundaries, and lack of resolution (mesh points).

Summarizing the discussion on Euler codes we may conclude that the problem of determining drag with acceptable accuracy is even more severe than for potential flow codes. In particular if distinction between wave drag and induced drag is the objective.

4.2.4 Zonal modelling

Assessing the various components of drag becomes more complicated when the effects of viscosity in the flow field are taken into account by matching the outer inviscid part of the flow field with the (inner) viscous or boundary layer part through an appropriate interaction law (zonal modelling). It appears, see Lighthill, Ref. 12, that there are several alternative ways for matching. However, the most convenient, and indeed most commonly adopted possibility, is to simulate the displacement effect of the boundary layer and wake on the outer inviscid flow through imposing a "transpiration mass flux" boundary condition on the body surface and wake centerline or vortex sheet. In the "weak" interaction formulation, which is applicable to attached flows only, the transpiration mass flux at the body surface and on the vortex sheet in the inviscid flow, and the tangential mass flux at the edge of the boundary layer in the boundary layer flow, are chosen such that the normal and tangential mass flux components in both the inviscid and boundary layer flow match at the location S_{edge}, figure 20, of the edge of the boundary layer and wake. In the "strong" interaction formulation, which is (also) applicable to separated flows, the sequence of "inviscid" and "viscous" calculations (interaction law) is chosen differently for reasons of computational stability and efficiency, with, however, the same objective of matching the inviscid and boundary layer flow at the edge of the boundary layer (see, e.g. Refs. 13, 14).

With zonal modelling in the sense described above, we have, in the inviscid part of the flow problem, apart from the actual inviscid flow outside the surface S_{edge}, an "equivalent" inviscid flow inside of S_{edge}. In the real viscous flow, the region within S_{edge} is, of course, occupied by the boundary layer and wake. In case the boundary layer and wake flow are modelled by the "classical" boundary layer equations there are no pressure gradients across the boundary layer and wake. However, triple deck theory for turbulent boundary layers (for a survey see, e.g. Ref. 14) teaches that normal pressure gradients are not negligible near the trailing edge, near separation lines and where shock waves intersect the boundary layer. The formulations given below are chosen such that they also cover the case with normal pressure gradients in the viscous flow.

With the purpose of relating "edge" and body/wake quantities we will now apply the momentum theorem first to the equivalent inviscid flow within S_{edge} (Fig. 20).
It reads

$$\oint\!\!\oint_{S_B+S_{wake}+S_{edge}+\delta S_{shock}+\delta S_{(\infty)}} [p\, n_x + (\rho\, \bar{q}.\bar{n})\, u]\, d\, S = 0 \qquad (15)$$

Note that, for the same reasons as discussed in sections 4.2.1 and 4.2.2 we have excluded the shock(s) from the area of integration.
Distinguishing the various parts of the area of integration eq. (15) can be written as

$$\underbrace{\oiint_{S_B} p\, n_x\, dS}_{D_{p_{eq.inv.}}} + \underbrace{\iint_{\delta S_{shock}} \left[p\, n_{1_x} + (\rho\, \bar{q}.\bar{n}_1)\, u \right]_2^1\, dS}_{-\delta I_{1,inv}} \;{}^{*)}$$

$$+ \underbrace{\iint_{S_{wake}} \left[p\, n_{1_x} + (\rho\, \bar{q}.\bar{n}_1)\, u \right]_2^1\, dS}_{-I_2} +$$

$$+ \underbrace{\iint_{S_{edge}+\,\delta S_{(\infty)}} p\, n_x\, dS}_{-D_{p_{edge}}} + \underbrace{\iint_{S_{edge}} (\rho\, \bar{q}.\bar{n})\, u\, dS}_{-I_{4,edge}} + \iint_{\delta S_{(\infty)}} \rho\, uu\, dS$$

$$+ \underbrace{\iint_{S_B} (\rho\, \bar{q}.\bar{n})\, u\, dS}_{-I_4} = 0 \qquad (16)$$

With the abbreviations introduced above, eq. (16) can be rewritten as

$$D_{p_{eq.inv}} - \delta I_{1,inv} - I_2 - I_4 + \iint_{\delta S_{(\infty)}} \rho\, uu\, dS = D_{p_{edge}} + I_{4,edge} \qquad (17)$$

or, making use of eq. (5), ($D_{p_{eq.inv}}$ of eq. (16), (17), being identical to D_p of eq. (5)),

$$I_1 - \delta I_{1,inv} + I_3 + \iint_{\delta S_{(\infty)}} \rho\, uu\, dS = D_{p_{edge}} + I_{4,edge} \qquad (18)$$

Eq. (18) relates the "far-field" and "edge" quantities of the "outer" inviscid flow.

We now apply the momentum theorem to the viscous flow within S_{edge} (Fig. 21). This gives

$$\oiint_{S_B + \delta S_{shock} + S_{edge} + \delta S_{(\infty)}} [p\, n_x + \tau_x + (\rho.\bar{q}.\bar{n})\, U]\, dS = 0 \qquad (19)$$

In eq. (19) τ_x represents the x-component of the frictional force, capital U the x-component of the total velocity in the viscous flow.
The total drag $D_{tot.}$ on the body can be written as

$$D_{tot.} = \oiint_{S_B} [p\, n_x + \tau_x]\, dS = D_{p_{visc}} + D_F \qquad (20)$$

or, using eq. (19)

$$D_{tot.} = \oiint_{S_B} (\rho\, \bar{q}.\bar{n})\, U\, dS +$$

$$\underbrace{- \iint_{\delta S_{shock}} \left[p\, n_{x_1} + \tau_{x_1} + (\rho\, \bar{q}.\bar{n}_1)\, U \right]_2^1\, dS}_{-\delta I_{1,visc}} +$$

$$- \iint_{S_{edge}} [p\, n_x + \overbrace{\tau_x}^{=0} + (\rho\, \bar{q}.\bar{n}_1)\, u]\, dS +$$

$$- \iint_{\delta S_{(\infty)}} [p + \tau_x + \overbrace{\rho\, UU}^{=0}]\, dS \qquad (21)$$

Note that in the case with normal pressure gradients the pressure drag in the viscous flow, $D_{p_{visc}}$, is not identical to the pressure drag in the equivalent inviscid flow $D_{p_{eq.inv}}$.

Note further that without mass transfer ($\rho\, \bar{q}.\bar{n} = 0$), and/or zero slip ($U = 0$), the first term of eq. (21) is zero.

---

*) As discussed in section 4.2.2 the smearing of shock waves by numerical schemes requires the jump integral δI_1, like I_1 itself, to be replaced by a (closed) contour integral.

Since $\tau_x = 0$ at the edge of the viscous region, and far downstream, and with the abbreviations introduced above, (see also eq. (16)), eq. (21) can be rewritten as

$$D_{tot.} = \delta I_{1,visc} + D_{p_{edge}} + I_{4,edge} - \iint_{\delta_{(\infty)}} \rho\, UU\, d\,S \tag{22}$$

or, using eq. (18)

$$D_{tot.} = I_1 - \delta,I_{1,inv} + \delta I_{1,visc} + I_3 + \iint_{\delta S_{(\infty)}} [\rho_{inv}\, uu - \rho\, UU]\, d\,S \tag{23}$$

where we have denoted the density of the equivalent inviscid flow within S_{edge} as ρ_{inv}, (u being the x-component of the total velocity of the equivalent inviscid flow).

It is worth noting at this point that the "shock correction" term $\delta I_{1,inv}$ (as well as I_1 itself) is zero in case of "Euler" type outer flow. Because (x-)momentum is conserved in the boundary layer flow we must also have $\delta I_{1,visc} = 0$ in case of matching with "Euler" flow. However, in case of matching with a "potential" outer flow model a conflict appears in the sense that (x-)momentum is conserved within the boundary layer but not at the edge, because momentum is not conserved across shock waves in potential flow. This suggests that $\delta I_{1,visc}$ is not necessarily zero in case of matching with a potential flow model, a point that deserves further attention and might be clarified by means of the theory of matched asymptotic expansions. In actual numerical calculations the shock, as mentioned before, is smeared over several meshes and both "shock correction" terms are usually ignored.

Returning to the expression (23) for the total drag we will now try to distinguish further between wave drag, vortex (or induced) drag, and viscous (boundary layer) drag and drag due to possible spurious residual sources within the flow field. For this purpose we first rewrite eq. (23) by introducing the expressions (7), (8) for I_1, the corresponding expressions for $\delta I_{1,inv}$, and (9) for I_3, giving

$$\begin{aligned} D_{tot} = {} & I_1' - \delta I_{1,inv}' + \delta I_{1,visc} + u_\infty\,(R_{shock} - \delta R_{shock}) \\ & - \oiint_{S_{(\infty)}} [p\, n_x + (u-u_\infty)\,(\rho\,\bar{q})_{inv}.\bar{n}]\, d\,S - u_\infty\, R_{(\infty)} + \\ & + u_\infty \oiint_{S_B+S_{wake}} (\rho\,\bar{q})_{inv}.\,\bar{n}\, d\,S + \iint_{\delta S_{(\infty)}} [\rho_{inv}\, uu - \rho\, UU]\, d\,S \end{aligned} \tag{24}$$

From the matching requirement that the mass fluxes outside the boundary layer and wake are equal in inviscid and viscous flow it follows that

$$\oiint_{S_{(\infty)}} (\rho\,\bar{q})_{inv}.\bar{n}\, d\,S - \iint_{\delta S_{(\infty)}} \rho_{inv}\, u\, d\,S = \overbrace{\oiint_{S_{(\infty)}} (\rho\,\bar{q})_{visc}.\,\bar{n}\, d\,S}^{=0} - \iint_{\delta S_{(\infty)}} \rho\, U\, d\,S \tag{25}$$

or, since, (eq. (10)),

$$\oiint_{S_{(\infty)}} (\rho\,\bar{q})_{inv}.\,\bar{n}\, d\,S = R_{(\infty)} - \oiint_{S_B+S_{wake}} (\rho\,\bar{q})_{inv}.\,\bar{n}\, d\,S \tag{26}$$

also that

$$\oiint_{S_B+S_{wake}} (\rho\,\bar{q})_{inv}.\,\bar{n}\, d\,S = R_{(\infty)} - \iint_{\delta S_{(\infty)}} (\rho_{inv}\, u - \rho\, U)\, d\,S \tag{27}$$

With (27), the expression (24) for the total drag finally takes the form

$$\begin{aligned} D_{tot.} = {} & I_1' - \delta I_{1,inv}' + \delta I_{1,visc} + u_\infty\,(R_{shock} - \delta R_{shock}) + \\ & \overbrace{- \oiint_{S_{(\infty)}} [p\, n_x + (u-u_\infty)(\rho\,\bar{q})_{inv}.\,\bar{n}]\, d\,S}^{I_3'} + \\ & \overbrace{+ \iint_{\delta S_{(\infty)}} (u-u_\infty)(\rho_{inv}\, u - \rho\, U)\, d\,S}^{I_5} + \\ & \overbrace{+ \iint_{\delta S_{(\infty)}} (u-U)\,\rho\, U\, d\,S}^{I_6} \end{aligned} \tag{28}$$

As before, we will consider the meaning of the various terms in eq. (28), in particular for the situation that the downstream boundary $(\delta)S_{(\infty)}$ of the control volume tends to infinity.

It follows from the preceeding discussions that in case the outer inviscid flow is modelled by the potential equation the wave drag is modelled by the terms $I_1'-\delta I_{1_{inv}}' + \delta I_{1_{visc}}$ and the induced drag by the term I_2'. Considering the term I_5 it may be noted that in two-dimensional flow $u \to u_\infty$ for $x \to \infty$, so that $I_5 \to 0$. In three dimensions with lift this is not exactly the case because of the flow perturbations induced by the trailing vortices. However, as indicated, a.o. by Lock (Ref. 10), the magnitude of the factor $(u-u_\infty)$, is generally negligible, except, perhaps for high lift and small aspect ratio. It is further noted, that the factor $(\rho_{inv}\, u-\rho U)$, when integrated over $\delta S_{(\infty)}$, is of the order of the displacement volume of the wake. Hence I_5, in all probability, can be safely neglected in most practical cases.
The term I_6, obviously, represents the viscous drag. We will return to this term in section 4.2.5.

In case the outer inviscid flow is modelled by means of the Euler equations we have, as mentioned before, $I_1-\delta I_{1_{inv}} + \delta I_{1_{visc}} = 0$, while I_2' contains both the induced drag and the wave drag of the equivalent inviscid flow. While $I_5 \to 0$ for potential flow, at least in two dimensions, it is, in general, $\neq 0$ in case of Euler flow because $u \neq u_\infty$ in the wake of shock waves. Hence, I_5, like the term(s) δI_1 in potential flow, can be considered as a (viscous) correction to the inviscid wave drag. It takes account of the fact that the wave drag associated with those parts of the shock waves of the equivalent inviscid flow within S_{edge} should be subtracted from the total "inviscid" wave drag. The author is not aware of any quantitative or numerical assessment of this term. The term I_6 again models the viscous drag.
It should be noted that if the downstream end of the control volume is taken at a finite distance from the configuration it is no longer possible to identify the various drag sources (induced/vortex, wave, viscous drag) directly and uniquely with the terms of eq. (28).

4.2.5 Viscous drag

As mentioned above, the viscous or boundary layer drag is represented by the term I_6 of eq. (28), or

$$D_{visc} = \iint_{\delta S_{(\infty)}} (u-U)\, \rho\, U\, d\, S \;(= I_6) \tag{29}$$

Evaluation of eq. (29) requires, in the general case, a method for the calculation of three-dimensional wakes. The problem is, however, that, even for planar, i.e. non-rolling-up wakes such methods are not generally available.
Limiting the discussions to wings, the approximate procedure that is usually followed to circumvent this problem is to compute the boundary layer, and, if possible, the wake, up to the trailing edge or some finite distance downstream of the trailing edge and to extrapolate the development of the viscous wake to downstream infinity.
For this purpose, eq. (29) is replaced by

$$D_{visc} = \rho_\infty u_\infty^2 \int_{S_{wake} \cap x=+\infty} \theta_\infty(y')\, dy' \tag{30}$$

where

$$\theta_\infty\,(y') = \int_{z'=-\infty}^{+\infty} \left(\frac{u}{u_\infty} - \frac{U}{u_\infty}\right) \frac{\rho U}{\rho_\infty\, u_\infty}\; dz' \tag{31}$$

is the (local) momentum thickness at downstream infinity. (y',z') are coordinates along and normal to the wake in the plane $x=+\infty$. Note that the expressions (30), (31) are applicable only in the case of planar, i.e. wing-like wakes.
In two-dimensional flow, the classical Squire and Young method (Ref. 15) or variants thereof are usually applied to relate θ_∞ to the momentum thickness $\theta(x)$ calculated by means of a boundary layer/wake method at some finite distance from the trailing edge. Under the assumption that the shape function H varies linearly with $\ln U_e$, (U_e being the velocity at the edge of the boundary layer), the Squire and Young method leads to the expression[e] (in "boundary layer" notation)

$$\theta_\infty = \theta(x) \left[\frac{T_e(x)}{T_e(\infty)}\right]^{\frac{1}{\gamma-1}} \left[\frac{U_e(x)}{U_e(\infty)}\right]^{2+\frac{H(x)+H(\infty)}{2}} \tag{32}$$

The procedure used for 3-D wings is generally similar to the one described above. In this case $\theta(x)$ is usually taken as θ_{TE} at the trailing edge and some extended form of the Squire and Young method, derived for infinite yawed wings, is used at each span station to relate θ_{TE} to θ_∞ (see e.g. Lock, Ref. 10).
It is appropriate at this point to stress the point that the basic assumptions underlying the Squire and Young method are not valid in case of (highly) asymmetric wakes (aft-loaded airfoils), wakes in (strong) pressure gradients and highly three-dimensional wakes. In such conditions methods of the type sketched above should be applied with caution.
Figures 22, 23 illustrate results of an application of the procedure to a 3D transport type wing and a comparison with experimental (wake rake) data (Ref. 16). A fully three-dimensional boundary layer code was used to calculate θ upto the trailing edge.
Figure 23 illustrates that even for a relatively simple case as that of figure 22 the difference between calculated and measured viscous drag may be substantial. Although there are numerous potential sources of error in, at least, the computational methods and procedures involved, the precise origin of such discrepancies is by no means clear.
An example of viscous drag prediction for a fairly complicated 2D case (airfoil with flap at low speed, from Ref. 17) is reproduced in figure 24. The figure serves the purpose of illustrating that turbulence modelling is of crucial importance for wakes in strong longitudinal pressure gradients such as occur in the main wake of flapped airfoils.

4.3 Cross-checking near-field and far-field values

In view of the inaccuracies and uncertainties discussed and illustrated above, it is advisable to compute the different components of drag in as many ways as possible and compare the results (viz. figure 25). Differences between drag component values computed in different ways may provide an indication of the error levels that are possibly involved.

On the inviscid side, an obvious check is to compare the integrated (near-field) pressure drag against the sum of the induced drag and wave drag as obtained from the (far-field) momentum considerations. Eq. (5) represents the basic equation for such a check.

In case of potential flow it may be more convenient to rewrite eq. (5) in terms of the expression (7), (8) and (9)-(13) for the (corrected) wave drag and induced drag.
This yields

$$D_{p_{eq.inv}} = I_1' + u_\infty R_{shock} + I_3' + u_\infty \left[\oiint_{S_B+S_{wake}} \rho\, \bar{q}.\bar{n}\, d\,S - R_{(\infty)} \right] - \iint_{S_{wake}} \left[p\, n_{1x} \right]_2^1 d\,S - \oiint_{S_B+S_{wake}} (\rho\, \bar{q}.\bar{n}) u\, d\,S \qquad (33)$$

or

$$D_{p_{eq.inv}} = D_{wave} + D_i + \overbrace{\oiint_{S_B+S_{wake}} (u_\infty - u)\, \rho\, \bar{q}.\bar{n}\, d\,S}^{D_{\delta^*}} + \overbrace{- \iint_{S_{wake}} \left[p\, n_{1x} \right]_2^1 d\,S}^{D_{p_{wake}}} - u_\infty [R_{(\infty)} - R_{shock}] \qquad (34)$$

with D_{wave} given by eq. (8) and D_i by eq. (11), (12) or (13). The third term on the right hand side of eq. (34), is non-zero in case of surface (and wake) "transpiration" only. It can be interpreted as the pressure drag (of the equivalent, inviscid flow) induced by the viscous displacement effect (D_{δ^*}). The fourth term, $D_{p_{wake}}$, represents the effect of a pressure jump across the inviscid wake discontinuity (vortex sheet). It is zero in case of a fully relaxed vortex sheet and vanishing viscous wake thickness or viscous wakes with zero normal pressure gradients (see also section 4.2.1). The terms $R_{(\infty)}$ and R_{shock} represent the effect of possible residual sources inside the flow field (section 4.2.2). They are, of course, zero in case of a fully converged solution.

In case the inviscid flow is modelled by the Euler equations it follows, from the discussion of sections 4.2.1 through 4.2.3, that the corresponding expression is

$$D_{p_{eq.inv}} = I_3' + \overbrace{\oiint_{S_B+S_{wake}} (u_\infty - u)\, \rho\, \bar{q}.\bar{n}\, d\,S}^{D_{\delta^*}} + \overbrace{- \iint_{S_{wake}} \left[p\, n_{1x} \right]_2^1 d\,S}^{D_{p_{wake}}} - u_\infty R_{(\infty)} \qquad (35)$$

with I_3' (eq. (11)) containing both the wave drag and the induced drag.

In viscous flow a similar check can, of course be performed by computing the total drag by integrating the surface pressure and skin friction, eq. (20), as well as by eq. (28).

An additional checking possibility is obtained by eliminating I_3' from eqs. (28) and (33), (34), leading to the general expression,

$$D_{p_{visc}} + D_F + \delta I_{1,inv}' - \delta I_{1,visc} + u_\infty \delta R_{shock} - I_5 - I_6 = D_{p_{eq.inv}} - D_{\delta^*} - D_{p_{wake}} + u_\infty R_{(\infty)} \qquad (37)$$

In case of potential outer flow we have $I_5 \approx 0$, at least in two dimensional flow (cf. section 4.2.4).
In case of "Euler" outer flow this reduces to

$$D_{p_{visc}} + D_F - I_5 - I_6 = D_{p_{eq.inv}} - D_{\delta^*} - D_{p_{wake}} + u_\infty R_{(\infty)} \qquad (38)$$

Note that, in the absence of shock waves, with zero normal pressure gradients across boundary layer and wake, and with zero mass flux residual, eqs. (37), (38) reduce further to

$$I_6\ (=D_{visc}) - D_F = D_{\delta^*} \tag{39}$$

expressing that the total viscous drag minus the friction drag equals (should equal), the pressure drag due to viscous effects.

4.4 Engineering approach to computational drag analysis

In the preceeding sections we have seen that we are still far from a situation in which we can compute drag with acceptable absolute accuracy. An additional problem is that the majority of the available inviscid flow codes provide values for integrated pressure drag only, so that a division into wave drag and induced drag is not readily available.

In spite of this situation it has proven to be possible to devise engineering procedures for determining drag from CFD codes with usable accuracy; at least in applications where drag increments, due to (small) changes in flow conditions or geometry, rather than absolute accuracy is the subject of interest. Examples of such procedures may be found in a.o. Refs. 3 and 18.

In Ref. 3 the induced drag of a wing-body configuration is calculated from Trefftz-plane considerations, utilizing the spanwise distribution of circulation obtained from a potential flow code and assuming that there is no vorticity shed from the body.

The following procedure is used to obtain an estimate for the wave drag. First, the total inviscid drag of the wing as determined from integrated pressures is compared with the induced drag of the wing for a number of subcritical flow conditions. Assuming that the induced drag is determined with sufficient accuracy this comparison yields a correction ΔC_{D_p} for the pressure drag which is expressed as a function of wing lift and Mach number as follows,

$$\Delta C_{D_p} = C_0 + C_2(C_{L_{wing}} + C_1)^2 + C_3 M_\infty^2 + C_4(1-M_\infty^2)^{-\frac{1}{2}} + C_5 M_\infty^2 C_{L_{wing}}^2 \tag{40}$$

The quadratic C_L-term in (40) is suggested by the fact that the induced drag (and hence, in subcritical flow, also the pressure drag) is a quadratic function of the lift; one would expect the error in this to be proportional to the level of the induced drag. The terms with M_∞^2 and $(1 - M_\infty^2)^{-\frac{1}{2}}$ are suggested by the Rayleigh-Janzen M_∞^2-expansion theory and Prandtl-Glauert theory, respectively. The cross-term $M_\infty^2 C_{L_{wing}}^2$ is merely empirical.

The constants C_0 to C_5 are determined by equating the corrected pressure drag and the far-field induced drag for six subcritical flow conditions involving three different C_L-values and three Mach numbers. The experience is that in this way the corrected pressure drag in the whole subcritical flow regime can be determined with an accuracy of a few drag counts. With the constants C_0 to C_5 known the correction formula (40) is also used to correct the pressure drag in supercritical flow conditions. For supercritical flow conditions the wave drag is then determined by subtracting the induced drag of the wing from the corrected pressure drag, i.e.

$$C_{D_{wave}} = C_{D_{p_{wing}}} + \Delta C_{D_p}(M_\infty, C_{L_{wing}}) - C_{D_{i_{wing}}} . \tag{41}$$

Note that the procedure assumes that wave drag is generated by the wing only.

An alternative for the "pressure drag error extrapolation" technique described above may be to use a mesh density extrapolation procedure of the type illustrated by figure 12.

The pressure drag error extrapolation procedure of Ref. 3 forms part of a fairly complex system of computer programs for the prediction of the aerodynamic characteristics of wing-body configuration in transonic flow (Fig. 26). In this system wing viscous drag is computed by a fully 3D finite difference type of boundary layer code in combination with an extended form of the Squire and Young method (section 4.2.5). Figure 27 provides comparisons of measured and computed drag for a narrow-body transport configuration, obtained through the system of figure 26, illustrating the usefulness of the drag prediction procedure. Note that the variation of drag with lift and Mach number is predicted reasonably well as long as the flow is attached; even the absolute drag level is fairly close if the computed wing drag is added to the (viscous) drag of the body alone as measured in the wind tunnel. Further examples may be found in ref. 3.

The pressure drag extrapolation technique may also be used wing section wise to obtain estimates for the distribution of wave drag along the span of the wing. Additional information provided by the system of figure 26 contains boundary layer and wing section viscous drag quantities (Fig. 28) and, of course, detailed pressure distributions.

5. COMPUTATIONAL DRAG MINIMIZATION

The past decade has seen repeated efforts, some (partly) succesful, others less so, to directly address the problem of drag minimization by combining computer codes for aerodynamic (drag) analyses (flow solvers) with numerical optimization algorithms. The objective being that the optimization algorithm controls variations of a number of independent variables, such as parameters defining the geometry, with the purpose of finding the particular combination of parameters that, subject to given constraints, leads to a minimal drag. In this process, the function of the flow solver is to provide drag values for each combination of values of the independent variables that is considered to be feasib e and "interesting" by the optimization algorithm.

Generally speaking computational (or numerical) drag minimization requires

- a choice of object function (in this case the drag, but other choices are possible)
- a flow solver (aerodynamic analysis code)
- a choice of independent variables
- a choice of constraint functions defining that part of the solution space that is considered to be feasible from the engineering or another (e.g. numerical) point of view

- an optimization algorithm.

With respect to the choice of independent variables one may distinguish two different approaches. One, and indeed the most common choice is to use parameters defining the geometry as the independent variables. This requires a direct or analyses type of flow solver only. The approach is generally referred to as direct numerical optimization.

While applications of the direct numerical optimization approach have seen the use of various aerodynamic codes, the feasible directions/gradient optimization algorithm COMMIN/COPES, developed by Vanderplaats (Ref. 19) seems to be used almost exclusively, in particular in combination with transonic flow codes.

The approach, pioneered by Hicks et al (Ref. 20) ows its existence entirely to the availability of large and fast computer systems. Because of the excessively large computational requirements, at least in 3D, the approach is sometimes referred to as "design by brute force". Nevertheless it holds great potential for the future. A reappraisal of the technique has been given by Hicks (Ref. 21). Several chastening experiences are also reported in Ref. 28.

A generalized flow diagram of the numerical optimization technique is presented in figure 29. The process is initiated by the choice of an aerodynamic object function F that is to be minimized (in this case the drag) a number of quantities to be constrained G_j and a set of design variables. The constraints can be of aerodynamic of geometric nature; e.g. C_L and/or t/c greater than a specified value. The design variables are generally taken to be the coefficients A_i of a number of shape functions

$$Z = Z_o + \sum_{i=1}^{n} A_i . f_i \qquad (42)$$

describing (modifications to) the starting wing geometry.

The process begins by perturbing, in sequence, each of the shape function coefficients A_i. The resulting n shapes are analyzed by means of the aerodynamic program (determination of F and G_j's) and the derivatives $\frac{\partial F}{\partial A_i}$, $\frac{\partial G_j}{\partial A_i}$, or rather the difference quotients $\frac{\Delta F}{\Delta A_i}$ $\frac{\Delta G_j}{\Delta A_i}$ are determined. The next step is the formation, by the optimization program, of the gradient ∇F and the determination of the direction of steepest descent of F, in the n-dimensional space formed by the basis vectors A_i, while satisfying the constraints. The optimization program then executes a number (typically 3) of steps in this direction, with another aerodynamic analysis performed at each step, until either a constraint is met or F attains a minimum. In the first case, or when the minimum of F is lower than the previous minimum, the process is repeated; new gradients are determined, etc. When the latest minimum or F is equal to or higher than the previous one the process is terminated.

The optimization process described above requires typically 10 complete cycles or, in other words, 10(n+3) analysis calculations (Ref. 19). This immediately illustrates the weakest point of the numerical optimization approach. In order to keep the computational effort required within reasonable bounds one has to put severe limitations on the number n of design variables, in particular in 3D flow. The problem is enhanced by the fact that for acceptable convergence of the optimization process it is necessary to avoid "numerical noise" in the partial derivates of the object function (Refs. 23, 24). This requires that the relaxation process in each analysis calculation must be continued until the residual has reached a level beyond that which is often customary in "normal" analysis calculations. It also appears to exclude the use of analysis codes with simple boundary layer corrections (Ref. 21). The reason for the latter is that the airfoil aerodynamic quantities do not vary consistently enough when boundary layer and potential flow are coupled in the weak interaction sense.

One way to reduce the number of analysis calculations required in 3D applications is to evolve the design variables in a series of steps (Ref. 26). For example by first designing the upper surface, section by section, going from root to tip and then the lower surface. Clearly it is also important to select a starting geometry having aerodynamic characteristics which are already close to the target. This asks for an information system/data base approach. With previous experience stored in the data base, the latter can be searched for the most suitable starting solution. As described in Ref. 19 the data base approach can also be used to speed-up the convergence of numerical optimization by at least a factor two. With the results of all preceding geometry perturbations stored it is possible to construct higher partial derivatives of the object function and utilize higher order gradient methods.

With the severe limitations on n, the choice of the shape functions is of utmost importance. The choice should be directed towards describing a sufficiently wide class of practical solutions. While simple polynomial expressions were used in early applications (Refs. 20, 22) of the numerical optimization concept, a more sophisticated class of shape functions describing more local geometry modifications was used in later applications, (Refs. 23, 24, 25). However, as discussed in Ref. 26, there is a need for still better shape functions with even more localized curvature variations. In fact it can be argued that while curvature based shape functions are suitable for areas with subcritical flow, slope based shape functions might be more appropriate in areas with locally supersonic flow.

An interesting choice for the shape functions is discussed by Aidala et.al. (Ref. 29). They consider shape functions generated by means of feeding certain pressure distribution modifications into an inverse program. The result is a set of design shapes that are (almost) orthogonal in an aerodynamic sense, that is, affect only one specific pressure distribution characteristic and no other ones.

While the choice of the design variables is of great practical significance, the precise choice of the object function, in conjunction with the choice of the aerodynamic and geometric constraints, is of both more fundamental and practical interest. In two-dimensional transonic applications (Refs. 19, 20, 22, 23) it has been customary to minimize the wave drag subject to constraints on, e.g., airfoil thickness or volume, lift and/or pitching moment. Although it is clear that constraints are necessary in a meaningful drag minimization problem it is by no means clear how exactly the problem should be formulated in order to guarantee a unique solution. The problem is illustrated by figure 30, taken from Ref. 19. Shown are the results of two drag minimization runs with identical free stream conditions and identical constraints on lift and airfoil volume. Only the starting solutions differ. As illustrated by the figure the two resulting airfoils are totally different in shape. Clearly the problem, as formulated, has more than one, local minimum and neither of the two necessarily represents the absolute minimum. An interesting discussion on criteria for suitable aerodynamic object functions can be found in Ref. 29.

Figure 30, the second airfoil in particular, also illustrates another potential problem of direct (inviscid) wave drag minimization. In the absence of (direct) control over the pressure distribution the solution may acquire unrealistically high pressure gradients, such as near the upper surface trailing edge.

A strong point of the numerical optimization approach is the possibility of selecting object functions and constraints suitable for multipoint designs. An example of a two-point design problem directed towards the design of airfoils with low drag creep can be found in Ref. 23. Low speed airfoil design applications are considered in Refs. 27, 30. It is also entirely possible to consider, e.g. transonic drag minimization and low-speed stall requirements simultaneously.

While the direct minimization of drag is feasible in two dimensions, it is hardly so, at present, in the case of three-dimensional wings. Several unsuccessful attempts in this direction can be found in the literature, (Refs. 24, 25, 26). The main reason for this failure is the lack of accuracy in the determination of the drag with the currently available 3D codes and the limited number of mesh points (Chapter 4). Another problem would seem to be that the problem of uniqueness in three dimensions is even more severe than in two dimensions. The accuracy problem may be overcome when more efficient algorithms and/or more computer power (vector/parallel machines) allows the number of mesh points to be increased. The uniqueness problem would probably require the introduction of more constraints or more sophisticated object functions.

Summarizing the discussion on direct numerical optimization, it may be said that the potential possibilities of the approach are enormous with, at present, unique capabilities such as multi-point and constrained design. However, the approach is also unique in terms of required computer resources. Substantial improvements in both flow optimization code algorithms and/or computer efficiency, relative to current general standards, are required before numerical optimization in 3D wing design can be used on a routine bases.

An alternative possibility for computational drag minimization is to use aerodynamic (load and pressure distribution) rather than geometric shape functions as independent variables. In this approach an optimization algorithm is used to optimize the pressure distribution, e.g. with the objective to minimize the drag. Using the latest available estimate of the geometry this can be done relatively cheap through an induced drag (Treffts plane) and a boundary layer code. While this approach implies direct control over induced drag and viscous drag it does not so with respect to wave drag. However, wave drag may be controlled indirectly by imposing constraints on the minimum pressure or maximum upper surface Mach number. With the target C_p-distribution established the new geometry can be determined by means of an inverse code. Subsequently the off-design characteristics can be determined by means of an analysis code. The process is repeated when the new geometry differs significantly from the previous one or when a geometry or off-design constraint is met. In the latter cases (new) constraints will have to be imposed on the values of the parameters describing the pressure distribution. A flow chart of the procedure, which is called inverse numerical optimization, (Ref. 31), is given by figure 31.

An example of a method which fits into the framework of inverse numerical optimization is one for determining the spanwise loadings for minimum induced drag on lifting parts of multiple, non-planar configurations (Ref. 32). The program utilizes constrained optimization techniques and panel method "technology" in the Treffts-plane. It is capable of dealing with pitching moment (trimmed situation) and bending moment constraints.

The input required by the program is summarized in figure 32. It comprises general geometric configuration data, position of the center of gravity, required (trimmed) lift coefficient, wing, body and tail pitching moment and drag data.

A typical example of the capabilities of the program is presented in figure 33. Figure 33a illustrates the type of configuration considered, with various vertical positions of the horizontal tail.

Optimum spanwise load distributions for a high and a low positioned horizontal tail for a given wing-body pitching moment and 30 % MAC c.g. location are compared in figure 33b. It illustrates the point that optimal wing design cannot be achieved without taking account of the tail configuration.

Minimum induced drag span loads for two different levels of wing-body pitching moment for a low tail configuration are compared in figure 33c. Figures 35d and e illustrate the point that the minimum trimmed induced drag of high tail configurations is much more sensitive to variations in wing-body pitching moment and c.g. positions than that of low tail configurations. This, however, does not necessarily imply that a low tail configuration is to be preferred; there may be other design criteria that dominate this choice.

In conclusion, figure 33f presents the optimum span load for a configuration which utilizes "active" loading of nacelle/pylon and flap rail fairings. In the particular example a 1.5 % reduction of the minimum trimmed induced drag can be realized by "active" rather than "passive" (streamline) shaping of pylons and flap rail fairings.

The program has been extended recently with an airfoil characteristics data base allowing e.g. the optimization of the spanwise distribution of wing section lift and pitching moment for minimum induced plus airfoil viscous drag for a given spanwise distribution of airfoil thickness.

Programs such as just described can be very helpful in the conceptual and preliminary design of minimum drag aircraft. They are also used for creating the starting point for the specification of "target" pressure distributions in the detailed aerodynamic design of wings by means of inverse methods.

Chordwise pressure distributions leading, approximately, to minimum viscous drag can, in principle, be determined by combining an optimization algorithm with a boundary layer code. Possibilities along these lines are currently being explored at NLR using a program system called CADOS (Ref. 33). The program uses basic "aerodynamic" as well as spline-type pressure distribution shape functions (Fig. 34) and can handle laminar as well as turbulent flows. It can address problems like the determination of the pressure distribution that, subject to constraints on, e.g. lift, pitching moment coefficient and average pressure level (airfoil thickness) leads to minimum viscous drag.

A simple, exploratory example of application is presented in figure 35. The figure shows the results of pressure distribution modifications to a basic pressure distribution by means of spline-type shape functions with the objective to minimize the drag. The boundary layer was not allowed to separate. Although the problem, as formulated, is not necessarily a sensible one, it illustrates the basic idea of the approach. In the particular case the answer is, obviously, determined to a large extent by the constraints implied by the basic and spline shape functions. Other choices for these will lead to a different answer. The approach is currently being explored further.

It is the author's opinion that the inverse numerical optimization approach is worthy of further investigation; not in the least because the computational effort required is much smaller than that of direct numerical optimization.

6 CONCLUDING REMARKS

An overview has been presented of the possibilities and problems associated with the prediction, analysis and minimization of drag using CFD methods. The discussion is limited to sub/transonic inviscid (potential and Euler) flow models, boundary layer and wake methods and methods employing viscous-inviscid interactions.

From the discussion it is concluded that the absolute accuracy of the computational determination of subsonic aircraft (wing) drag is, currently, of the order of 10 to 30 "counts" at best. The main problems seem to be

- lack of resolution due to the limited number of mesh-points and lack of convergence due to the limited number of iterations or time steps that can be run on the computer systems that are currently available in most engineering environments (particular important for wave drag and, but possibly to a lesser extent, for induced drag)
- spurious entropy production in Euler codes as a result of insufficiently accurate implementation of boundary conditions
- lack of (appropriate) methods and turbulence models for the computation of wakes in pressure gradient and boundary layers with complex interaction phenomena.

An additional problem of the majority of the available inviscid flow codes is that they provide values for integrated pressure drag only so that a division into wave drag and induced drag is not readily available. In spite of this situation it has proved possible to devise engineering procedures for determining drag increments for (closely) similar flow conditions or configurations with usable accuracy.

Closely related to the problems mentioned above is the fact that configuration optimization for drag reduction by means of direct numerical optimization techniques is hardly feasible in current engineering environments, at least for three-dimensional problems. An alternative might be to use numerical optimization for designing minimum drag "target" pressure distributions and to use inverse methods to find the corresponding geometry (inverse numerical optimization).

Summarizing, it may be stated the accurate numerical determination and minimization of drag is currently almost "mission impossible", at least for three-dimensional flow. However, there are exciting prospects for the future, not in the least because of the continuing rapid advancements in computer technology.

REFERENCES

No.	Author	Title, etc.
1	Salas, M.D. Jameson, A. Melnik, R.E.	A comparative study of the non-uniqueness problem of the potential equation AIAA-83-1888
2	Yoshihara, H. (editor)	Report of WG07 on test cases for inviscid flow field methods AGARD Rept. 211, 1985
3	v.d. Vooren, J. v.d. Kolk, J.Th. Slooff, J.W.	A system for the numerical simulation of sub- and transonic viscous attached flows around wing-body configurations. AIAA-82-0935, 1982
4	de Bruin, A.C.	Unpublished work, NLR, 1983
5	v.d. Berg, B.	Unpublished work, NLR, 1983
6	Steger, J.L. Baldwin, B.S.	Shock waves and drag in the numerical calculation of isentropic transonic flow NASA TN D-6997, 1972
7	v.d. Vooren, J. Slooff, J.W.	On isentropic flow models used for finite difference calculations of two-dimensional transonic flows with embedded shocks NLR MP 73024 U, 1983
8	Yu, N.J. Chen, H.C. Samant, S.S. Rubbert, P.E.	Inviscid drag calculations for transonic flows AIAA-83-1928
9	Garabedian, P. McFadden, G.	Computational fluid dynamics of airfoils and wings, in: Proceedings of Symposium on Transonic Shock and Multi-Dimensional Flows: Advances in Scientific Computing, ed. R. Meyer, Academic Press, N.Y. 1982
10	Lock, R.C.	Prediction of the drag of wings at subsonic speeds by viscous/inviscid interaction techniques AGARD Lecture Series on "Drag Prediction and Reduction", 1985
11	Oswatitsch, K.	Der Verdichtungsstoss bei der stationären Umströmung flacher Profile, ZAMM 29, 129-141, 1949
12	Lighthill, M.J.	On displacement thickness J.Fl.Mech. 4, p. 383, 1958

13	Le Balleur, J.C.	La Recherche Aerospacial (ONERA), 1981-3,21 1981
14	Melnik, R.	Turbulent interactions on airfoils at transonic speeds - recent developments AGARD CP No. 291, paper 10, 1980
15	Squire, H.B. Young, A.D.	The calculation of the profile drag of aerofoils A.R.C. R&M 1838, 1937
16	Elsenaar, A.	Unpublished work, NLR
17	Oskam, B.	Recent advances in computational methods to solve the high-lift multi-component airfoil problem AGARD CP.365, 1984, also NLR MP 84042 U
18	Henne, P.A. Dahlin, J.A. Peavey,C.C.	Applied computational transonics - capabilities and limitations In: Transonic Aerodynamics, Progress in Astronautics and Aeronautics, Vol. 81 AIAA, N.Y. 1982
19	Vanderplaats, G.N.	An efficient algorithm for numerical airfoil optimization AIAA-79-0079, 1979
20	Hicks, R.M. Murman, E.M. Vanderplaats, G.N.	An assessment of airfoil design by numerical optimization, NASA TM X-30092, 1974
21	Hicks, R.M.	Transonic wing design using potential flow codes - Successes and failures SAE Paper 810565, 1981
22	Hicks, R.M. Vanderplaats, G.N. Murman, E.M. King, Rosa T.	Airfoil section drag reduction at transonic speeds by numerical optimization SAE Paper 760477, 1976
23	Hicks, R.M. Vanderplaats, G.N.	Application of numerical optimization to the design of supercritical airfoils without drag-creep, SAE Paper 770440, 1977.
24	Hicks, R.M. Henne, P.A.	Wing design by numerical optimization AIAA Paper No. 77-1247, 1977
25	Haney, H.P. Johnson, R.R. Hicks, R.M.	Computational optimization and wind-tunnel test of transonic wing designs AIAA Paper No. 79-0080, 1979.
26	Lores, M.E. Smith, P.E. Large, R.A.	Numerical optimization: an assessment of its role in transport aircraft aerodynamic design through a case study, ICAS-80-1.2, 1980
27	Hicks, R.M. Vanderplaats, G.N.	Design of low-speed airfoils by numerical optimization SAE Paper 750524, 1975
28	Nixon, D. (editor)	Transonic aerodynamics, Progress in Astronautics and Aeronautics, Vol. 81 AIAA, N.Y. 1982
29	Aidala, P.V. Davis, W.H. Mason, W.H.	Smart aerodynamic optimization AIAA-83-1836, 1983
30	Misegades, K.P.	Airfoil optimization AIAA-84-0053, January 1984
31	Slooff, J.W.	Computational methods for subsonic and transonic aerodynamic design In: Special Course on Subsonic/Transonic Aerodynamic Interference for Aircraft AGARD Rept. No. 712, 1983
32	Van den Dam, R.F.	SAMID, an interactive system for the analysis and constrained minimization of induced drag, AIAA-83-0095, 1983
33	Boerstoel, J.W. v. Egmond, J.A. Kassies, A. Slooff, J.W.	Unpublished work, NLR

- NORMAL (PRESSURE) FORCES

→ PRESSURE DRAG

- TANGENTIAL (FRICTION) FORCES

→ FRICTION DRAG

Fig. 1 Distinction of drag components according to type of force

- FRICTION

→ "VISCOUS" OR "BOUNDARY LAYER" DRAG

(FRICTION + PRESSURE FORCES)

- VORTEX SHEDDING

→ "INDUCED" OR "VORTEX" DRAG

(PRESSURE DRAG ONLY)

- SHOCK WAVE FORMATION

→ WAVE DRAG

(PRESSURE DRAG ONLY)

Fig. 2 Distinction of drag components according to the responsible physical mechanisms

(SUBSONIC) MINIMUM DRAG

CONTAINS:

- (MOST OF) VISCOUS DRAG
- (SOME) INDUCED DRAG

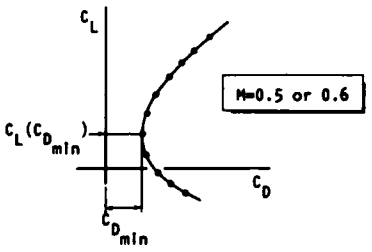

- USUALLY ESTIMATED BY MEANS OF FORM FACTOR METHODS

$$C_{D_{min}} = C_F(1 + k\ t/c + \ldots)\ .\frac{S_{wet}}{S_{ref}}$$

Fig. 3 Definition of "(subsonic) minimum drag"

(SUBSONIC) DRAG-DUE-TO-LIFT

CONTAINS:

- (MOST OF) INDUCED DRAG
- (SOME) VISCOUS DRAG
- (POSSIBLY SOME WAVE DRAG)

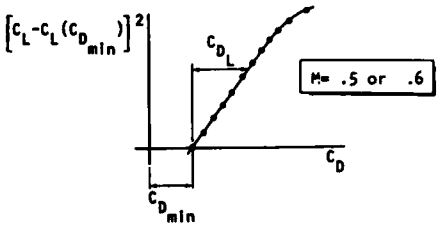

- USUALLY ESTIMATED OR FITTED BY MEANS OF CLASSICAL INDUCED DRAG FORMULA

$$C_{D_L} = \frac{\left[C_L - C_L(C_{D_{min}})\right]^2}{\pi Ae}$$

Fig. 4 Definition of "drag due to lif "

COMPRESSIBILITY DRAG

CONTAINS:

- MOST IF NOT ALL WAVE DRAG
- SOME VISCOUS DRAG
- SOME INDUCED DRAG

(DUE TO CHANGE IN SPAN LOADING WITH MACH NUMBER)

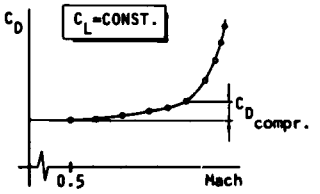

- NO GENERAL THEORETICAL BASIS FOR PREDICTION

Fig. 5 Definition of "compressibility drag"

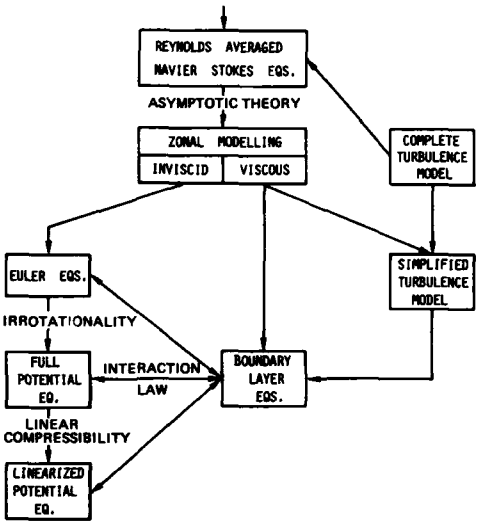

Fig. 6 Hierarchy of mathematical/physical CFD flow models

- (REYNOLDS AVERAGED) NAVIER - STOKES METHODS
  - CAN PROVIDE FRICTION DRAG AND PRESSURE DRAG
  - CONTAIN ALL INFORMATION NECESSARY TO DISTINGUISH BETWEEN VISCOUS DRAG, INDUCED DRAG AND WAVE DRAG
  - GENERALLY NOT YET AVAILABLE IN *INDUSTRIAL ENVIRONMENT*
- INVISCID METHODS
  - MODEL PRESSURE DRAG ONLY

	INDUCED DRAG	WAVE DRAG
EULER	X	X
FULL POTENTIAL	X	X *)
LINEARIZED POTENTIAL	X	-

*) APPROXIMATIVE, ACCEPTABLY ACCURATE FOR $M_n < 1.3$?

- BOUNDARY LAYER AND WAKE METHODS
  - FRICTION DRAG (BOUNDARY LAYER)
  - TOTAL VISCOUS DRAG (WAKE)

Fig. 7 Drag (component) prediction capability potential of various CFD models

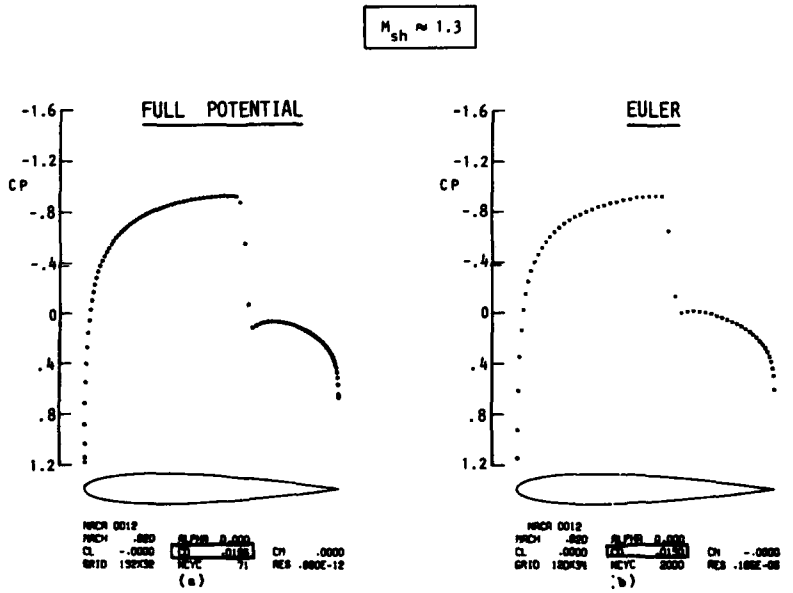

Fig. 8 Comparison of Euler (FLO52S) and full potential (FLO36) solutions (Ref. 1)

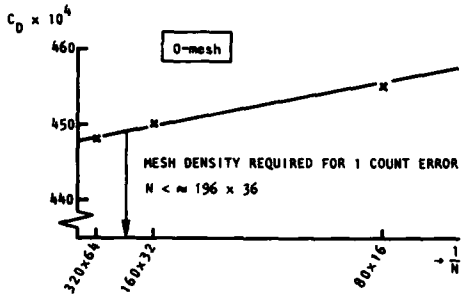

Fig. 9 Example of pressure drag dependence on mesh density (Euler code, RAE 2822 airfoil, M = 0.75, α = 3°, strong shock)

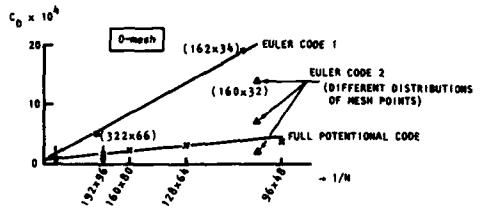

Fig. 10 Example of pressure drag dependence on mesh density and mesh distribution (shock-free supercritical airfoil, NLR 7301)

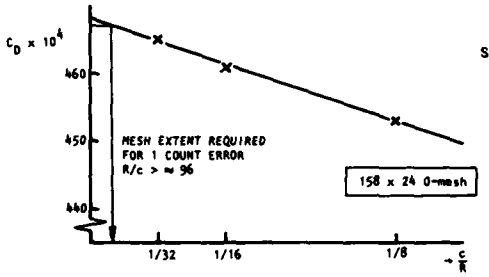

Fig. 11 Example of pressure drag dependence on mesh extent (Euler code, RAE 2822, M = 0.75, α = 3°, strong shock)

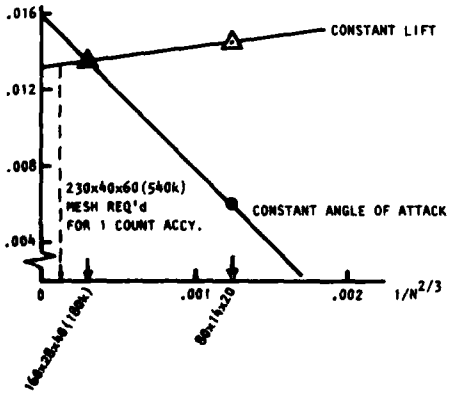

Fig. 12 Example of pressure drag as a function of mesh density for a transport type wing with transonic flow ((K)FLO22 program)

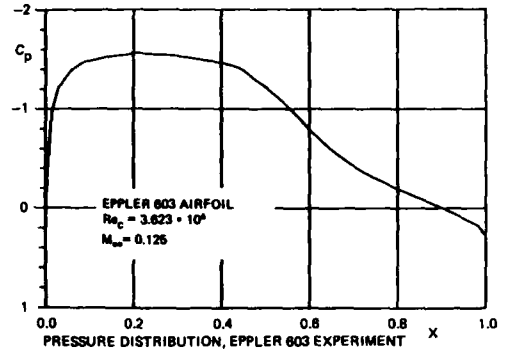

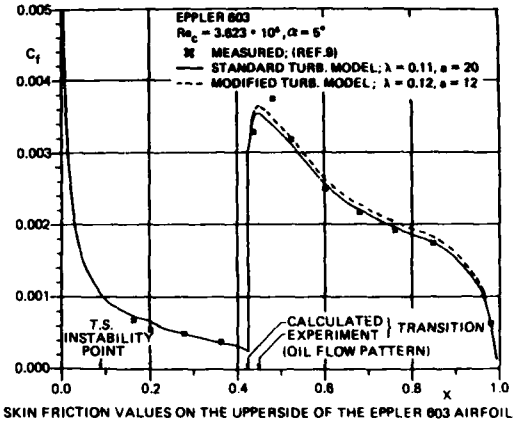

Fig. 13 Example of skin friction prediction (I) (from ref. 4)

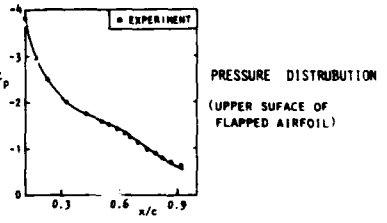

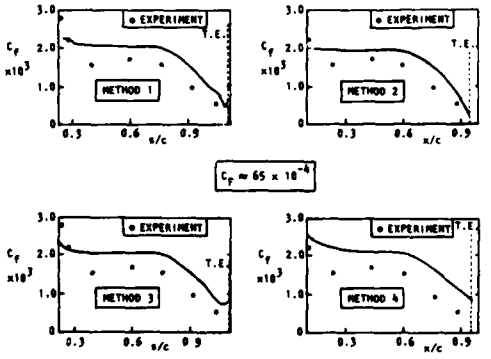

Fig. 14 Example of friction drag prediction (II) (from ref. 5)

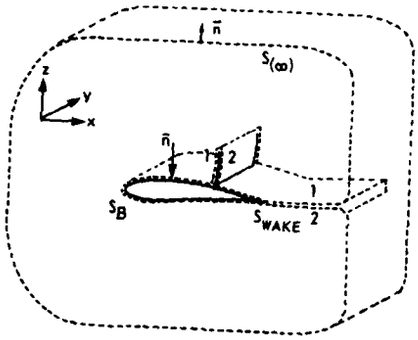

Fig. 15 Control volume for determination of (inviscid) drag through application of momentum theorem

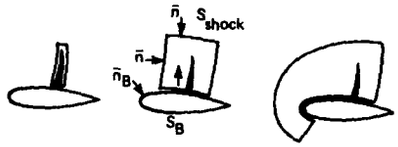

Fig. 16 Permissible contours of integration for wave drag calculation in potential flow

SURFACE GRIDS (MODIFIED FL028 CODE)

Contours \ Iterations	100	500	1000
	0.0061	0.0059	0.0059
	0.0039	0.0035	0.0034
	0.0051	0.0046	0.0046
	0.0048	0.0044	0.0044

Fig. 17 Wave drag calculations for a transport wing-body configuration at $M_\infty = 0.84$, $\alpha = 2.73$ deg (Ref. 8)

$$D_i = \int_{S_{wake} \cap x=\infty} [\phi]\,\bar{q}.\bar{n}_{wake}\,dt$$

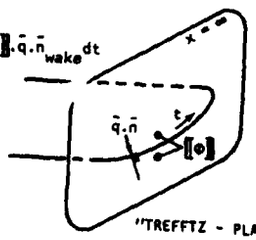

Fig. 18 Calculation of induced drag from Treffts-plane integration

OSWATISCH DRAG FORMULA

$$D = \frac{T_\infty}{q_\infty} \int_{S_{shock}} (\tilde{S}-\tilde{S}_\infty)\rho\bar{q}.\bar{n}\,dS$$

($\tilde{S}$ IS ENTROPY)

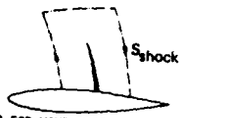

CONTOUR FOR WAVE DRAG CALCULATION FROM ENTROPY PRODUCTION IN EULER CODE

Fig. 19 Evaluation of wave drag from entropy production (Euler codes)

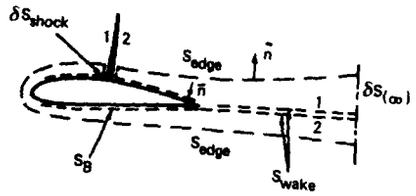

Fig. 20 Zonal modelling; the inviscid part of the problem

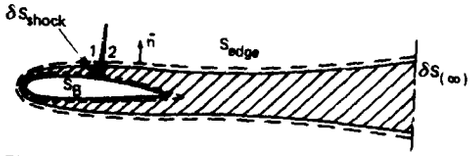

Fig. 21 Zonal modelling; the viscous part of the problem

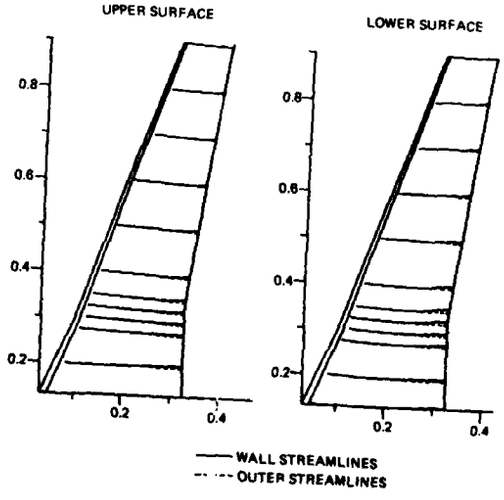

Fig. 22 Wing planform (transport type wing) plus outer- and wall streamlines from 3D boundary layer calculations ($M_\infty = 0.5$, $Re_c = 2.10^6$)

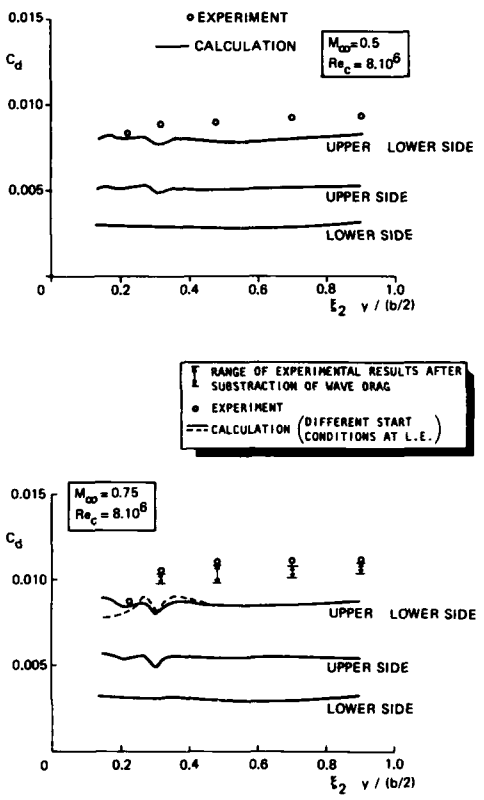

Fig. 23 Comparison of experimental (wake rake) and calculated viscous drag distribution for transport type wing

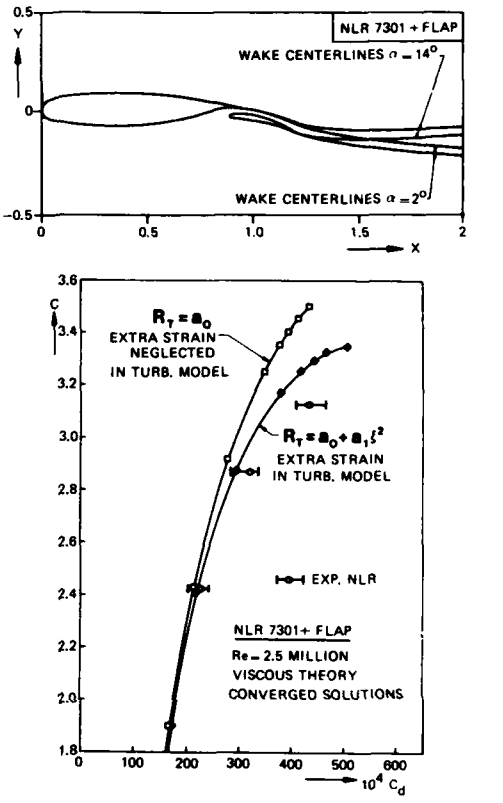

Fig. 24 Effect of turbulence model on lift/drag in case of wake with strong longitudinal pressure gradient

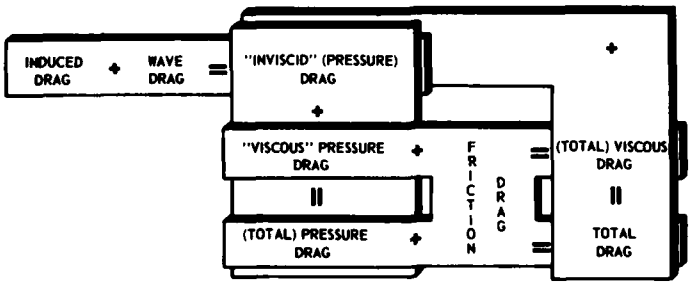

Fig. 25 Chart of relations between drag components

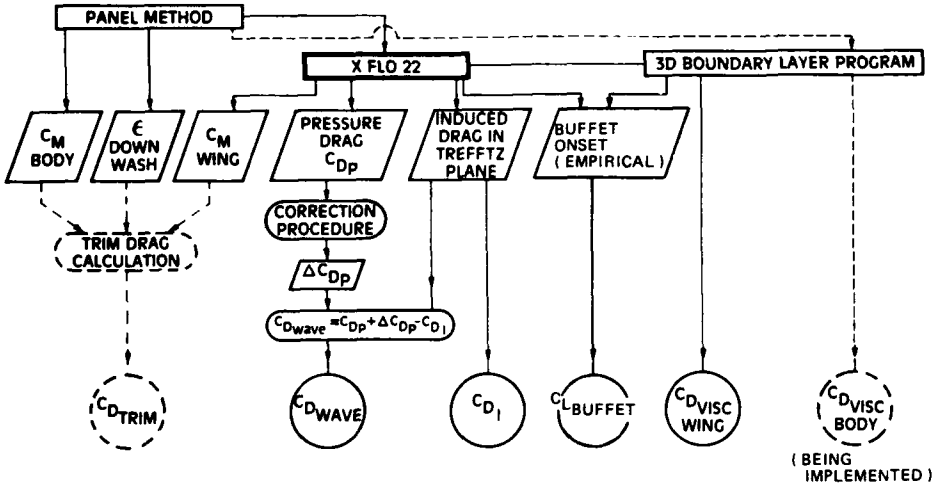

Fig. 26 Schematic of NLR XFLO22 system for the analysis of wing-fuselage configurations in transonic flow

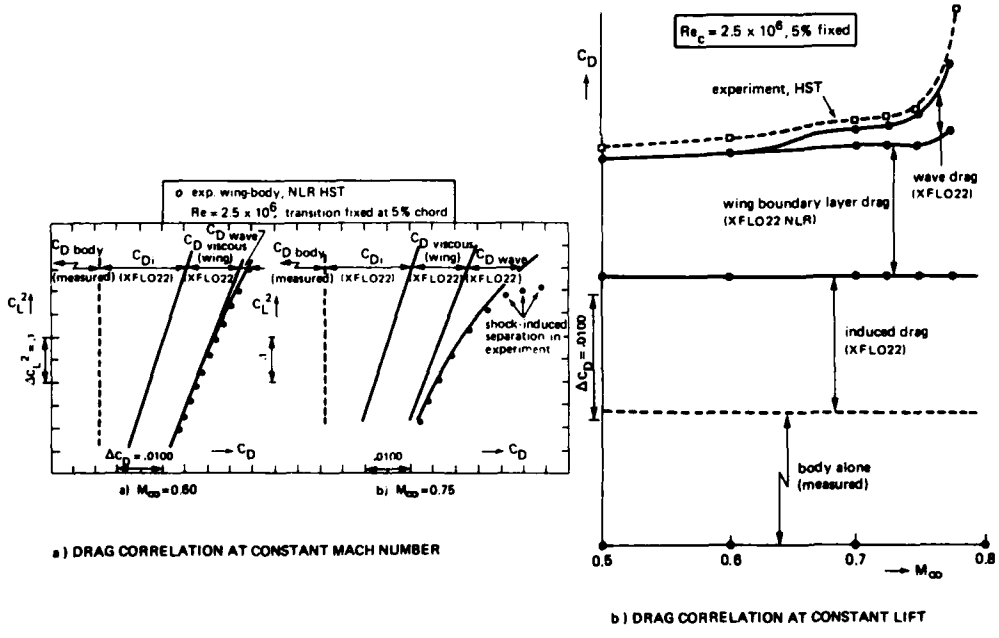

Fig. 27 NLR XFLO22 drag analyses fo narrow-body transport configuration

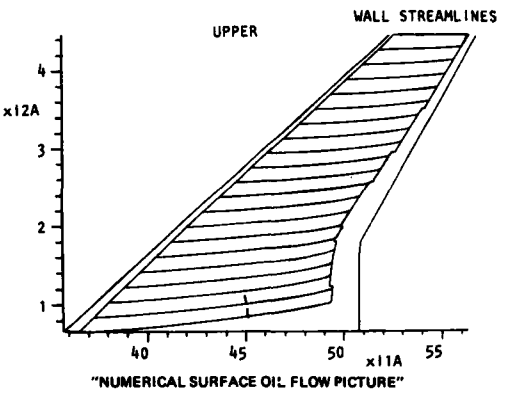

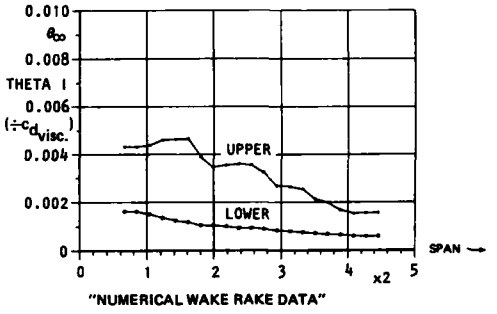

Fig. 28 NLR XFLO22 wing-fuselage transonic analysis system: examples of standard graphics output

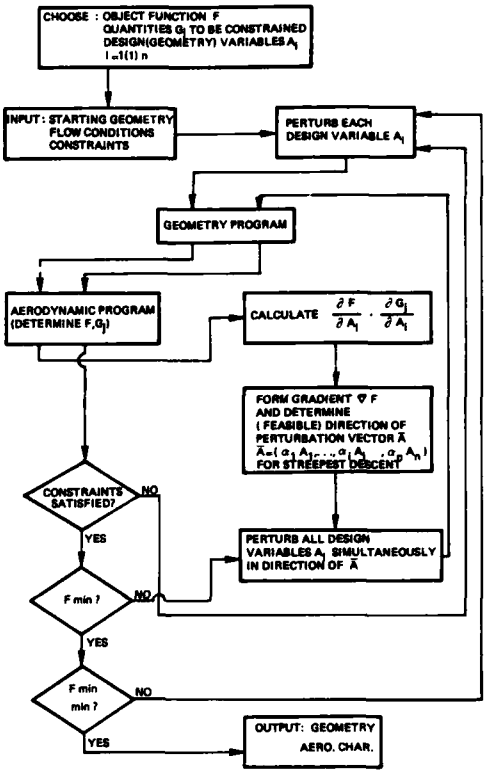

Fig. 29 Flow chart of direct numerical optimisation

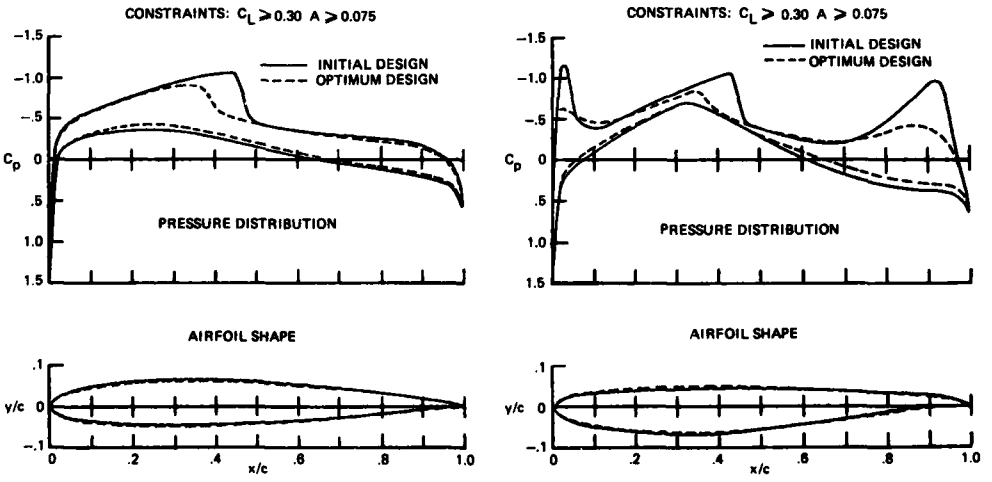

Example 3A–drag minimization, M = 0.75, $\alpha = 0^\circ$, beginning analysis No. 27.

Example 3B–drag minimization, M = 0.75, $\alpha = 0^\circ$, beginning with analysis No. 48.

Fig. 30 Example of non-uniqueness of wave drag minimization problem

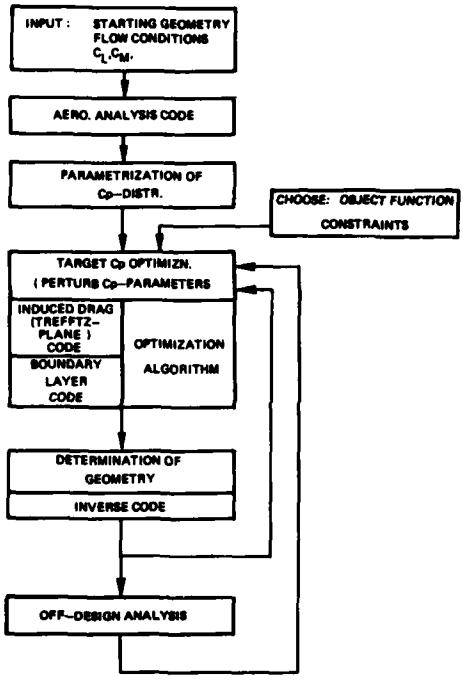

Fig. 31 Scheme for inverse numerical optimisation (conjectural)

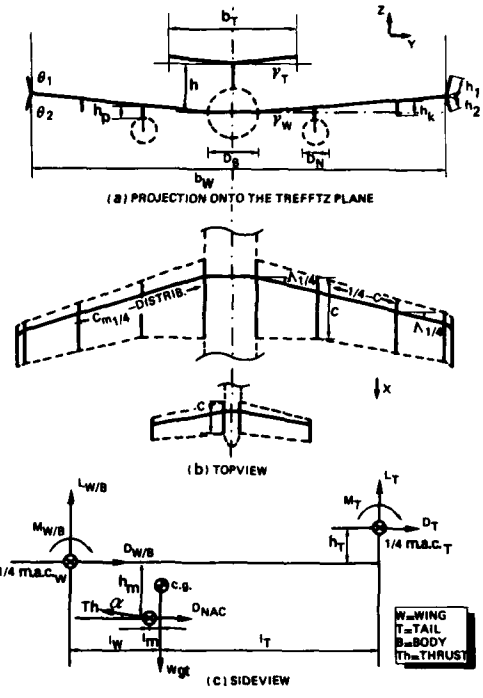

Fig. 32 Summary of input parameters for trimmed induced drag minimization

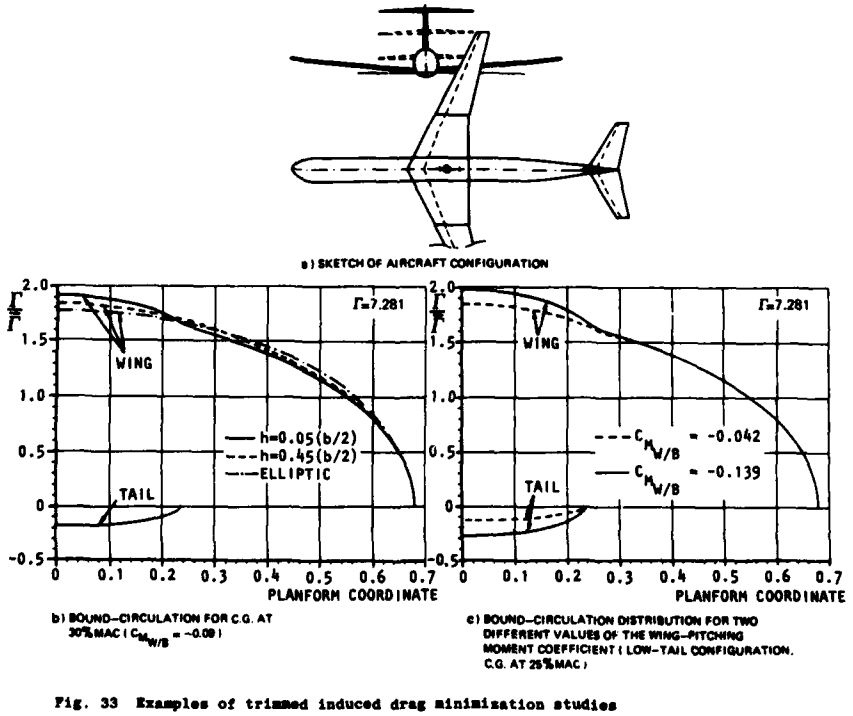

Fig. 33 Examples of trimmed induced drag minimization studies

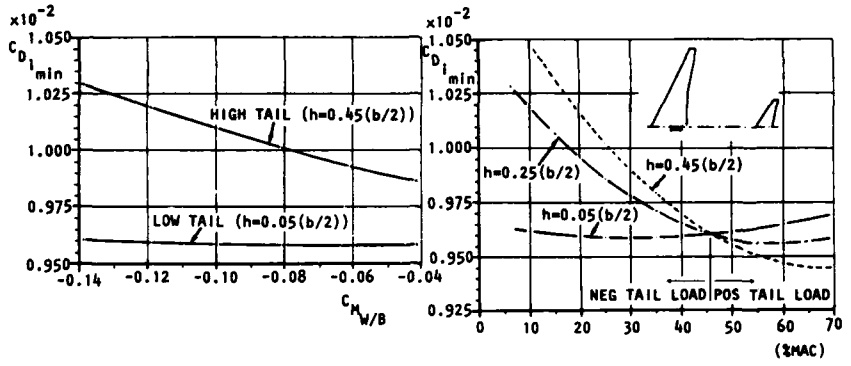

d) INFLUENCE OF THE WING/BODY PITCHING MOMENT COEFFICIENT $C_{M_{W/B}}$ ON THE MINIMUM TRIMMED INDUCED-DRAG (C_{M_B} = 0.007 , C.G. AT 25%MAC)

e) EFFECTS OF THE LOCATION OF CENTER OF GRAVITY AND THE TAIL HEIGHT RELATIVE TO THE WING ON THE MINIMUM TRIMMED INDUCED- DRAG ($C_{M_{W/B}} = -0.05$)

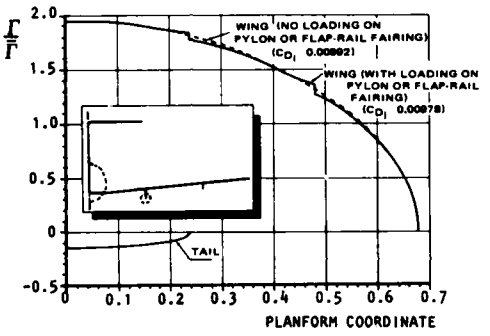

f) THE AIRCRAFT CONFIGURATION WITH PYLON/NACELLE AND FLAP-RAIL FAIRINGS, DESIGNED FOR MINIMUM TRIMMED INDUCED DRAG (C.G. AT 32%MAC)

Fig. 33 Examples of trimmed induced drag minimization studies (continued)

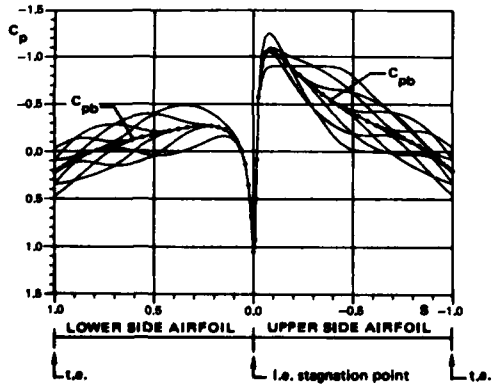

Fig. 34 Spline shape functions and basic pressure distribution C_{pB} for pressure-distribution optimization

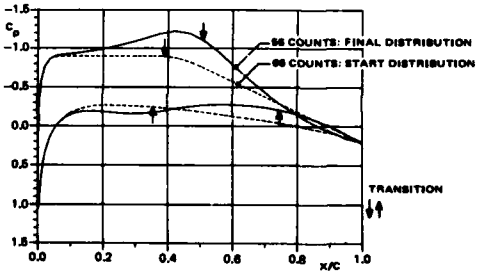

Fig. 35 Result of constrained drag minimization with spline shape functions

REPORT DOCUMENTATION PAGE			
1. Recipient's Reference	**2. Originator's Reference** AGARD-R-723 Addendum	**3. Further Reference** ISBN 92-835-1524-2	**4. Security Classification of Document** UNCLASSIFIED

5. Originator Advisory Group for Aerospace Research and Development
North Atlantic Treaty Organization
7 rue Ancelle, 92200 Neuilly sur Seine, France

6. Title

AIRCRAFT DRAG PREDICTION AND REDUCTION

7. Presented at

8. Author(s)/Editor(s)	**9. Date**
J.W.Slooff	April 1986
10. Author's/Editor's Address National Aerospace Laboratory (NLR) Amsterdam Netherlands	**11. Pages** 30

12. Distribution Statement This document is distributed in accordance with AGARD policies and regulations, which are outlined on the Outside Back Covers of all AGARD publications.

13. Keywords/Descriptors

Aerodynamic drag	Turbulence
Laminar flow	External stores
Skin friction	Nacelles
Boundary layer	

14. Abstract

The Special Course on Aircraft Drag Prediction was sponsored by the AGARD Fluid Dynamics Panel and the von Kármán Institute and presented at the von Kármán Institute, Rhode-Saint-Genèse, Belgium, on 20—23 May 1985 and at the NASA Langley Research Center, Hampton, Virginia, USA, 5—9 August 1985.

The course began with a general review of drag reduction technology. Then the possibility of reduction of skin friction through control of laminar flow and through modification of the structure of the turbulence in the boundary layer were discussed. Methods for predicting and reducing the drag of external stores, of nacelles, of fuselage protuberances, and of fuselage afterbodies were then presented followed by discussion of transonic drag rise. The prediction of viscous and wave drag by a method matching inviscid flow calculations and boundary layer integral calculations, and the reduction of transonic drag through boundary layer control are also discussed.

This volume comprises Paper No.9 "Computational Drag Analyses and Minimization: Mission Impossible?" which was not included in AGARD Report 723 (main volume).

AGARD Report No.723 Addendum Advisory Group for Aerospace Research and Development, NATO AIRCRAFT DRAG PREDICTION AND REDUCTION Published April 1986 by J.W.Slooff 30 pages The Special Course on Aircraft Drag Prediction was sponsored by the AGARD Fluid Dynamics Panel and the von Kármán Institute and presented at the von Kármán Institute, Rhode-Saint-Genèse, Belgium, on 20—23 May 1985 and at the NASA Langley Research Center, Hampton, Virginia, USA, 5—9 August 1985. The course began with a general review of drag reduction technology. Then the possibility of reduction of skin friction P.T.O	AGARD-R-723 Addendum 1 Aerodynamic drag Laminar flow Skin friction Boundary layer Turbulence External stores Nacelles	AGARD Report No.723 Addendum Advisory Group for Aerospace Research and Development, NATO AIRCRAFT DRAG PREDICTION AND REDUCTION Published April 1986 by J.W.Slooff 30 pages The Special Course on Aircraft Drag Prediction was sponsored by the AGARD Fluid Dynamics Panel and the von Kármán Institute and presented at the von Kármán Institute, Rhode-Saint-Genèse, Belgium, on 20—23 May 1985 and at the NASA Langley Research Center, Hampton, Virginia, USA, 5—9 August 1985. The course began with a general review of drag reduction technology. Then the possibility of reduction of skin friction P.T.O	AGARD-R-723 Addendum 1 Aerodynamic drag Laminar flow Skin friction Boundary layer Turbulence External stores Nacelles
AGARD Report No.723 Addendum Advisory Group for Aerospace Research and Development, NATO AIRCRAFT DRAG PREDICTION AND REDUCTION Published April 1986 by J.W.Slooff 30 pages The Special Course on Aircraft Drag Prediction was sponsored by the AGARD Fluid Dynamics Panel and the von Kármán Institute and presented at the von Kármán Institute, Rhode-Saint-Genèse, Belgium, on 20—23 May 1985 and at the NASA Langley Research Center, Hampton, Virginia, USA, 5—9 August 1985. The course began with a general review of drag reduction technology. Then the possibility of reduction of skin friction P.T.O	AGARD-R-723 Addendum 1 Aerodynamic drag Laminar flow Skin friction Boundary layer Turbulence External stores Nacelles	AGARD Report No.723 Addendum Advisory Group for Aerospace Research and Development, NATO AIRCRAFT DRAG PREDICTION AND REDUCTION Published April 1986 by J.W.Slooff 30 pages The Special Course on Aircraft Drag Prediction was sponsored by the AGARD Fluid Dynamics Panel and the von Kármán Institute and presented at the von Kármán Institute, Rhode-Saint-Genèse, Belgium, on 20—23 May 1985 and at the NASA Langley Research Center, Hampton, Virginia, USA, 5—9 August 1985. The course began with a general review of drag reduction technology. Then the possibility of reduction of skin friction P.T.O	AGARD-R-723 Addendum 1 Aerodynamic drag Laminar flow Skin friction Boundary layer Turbulence External stores Nacelles

through control of laminar flow and through modification of the structure of the turbulence in the boundary layer were discussed. Methods for predicting and reducing the drag of external stores, of nacelles, of fuselage protuberances, and of fuselage afterbodies were then presented followed by discussion of transonic drag rise. The prediction of viscous and wave drag by a method matching inviscid flow calculations and boundary layer integral calculations, and the reduction of transonic drag through boundary layer control are also discussed.

This volume comprises Paper No.9 "Computational Drag Analyses and Minimization: Mission Impossible?" which was not included in AGARD Report 723 (main volume).

ISBN 92-835-1524-2

through control of laminar flow and through modification of the structure of the turbulence in the boundary layer were discussed. Methods for predicting and reducing the drag of external stores, of nacelles, of fuselage protuberances, and of fuselage afterbodies were then presented followed by discussion of transonic drag rise. The prediction of viscous and wave drag by a method matching inviscid flow calculations and boundary layer integral calculations, and the reduction of transonic drag through boundary layer control are also discussed.

This volume comprises Paper No.9 "Computational Drag Analyses and Minimization: Mission Impossible?" which was not included in AGARD Report 723 (main volume).

ISBN 92-835-1524-2

through control of laminar flow and through modification of the structure of the turbulence in the boundary layer were discussed. Methods for predicting and reducing the drag of external stores, of nacelles, of fuselage protuberances, and of fuselage afterbodies were then presented followed by discussion of transonic drag rise. The prediction of viscous and wave drag by a method matching inviscid flow calculations and boundary layer integral calculations, and the reduction of transonic drag through boundary layer control are also discussed.

This volume comprises Paper No.9 "Computational Drag Analyses and Minimization: Mission Impossible?" which was not included in AGARD Report 723 (main volume).

ISBN 92-835-1524-2

through control of laminar flow and through modification of the structure of the turbulence in the boundary layer were discussed. Methods for predicting and reducing the drag of external stores, of nacelles, of fuselage protuberances, and of fuselage afterbodies were then presented followed by discussion of transonic drag rise. The prediction of viscous and wave drag by a method matching inviscid flow calculations and boundary layer integral calculations, and the reduction of transonic drag through boundary layer control are also discussed.

This volume comprises Paper No.9 "Computational Drag Analyses and Minimization: Mission Impossible?" which was not included in AGARD Report 723 (main volume).

ISBN 92-835-1524-2

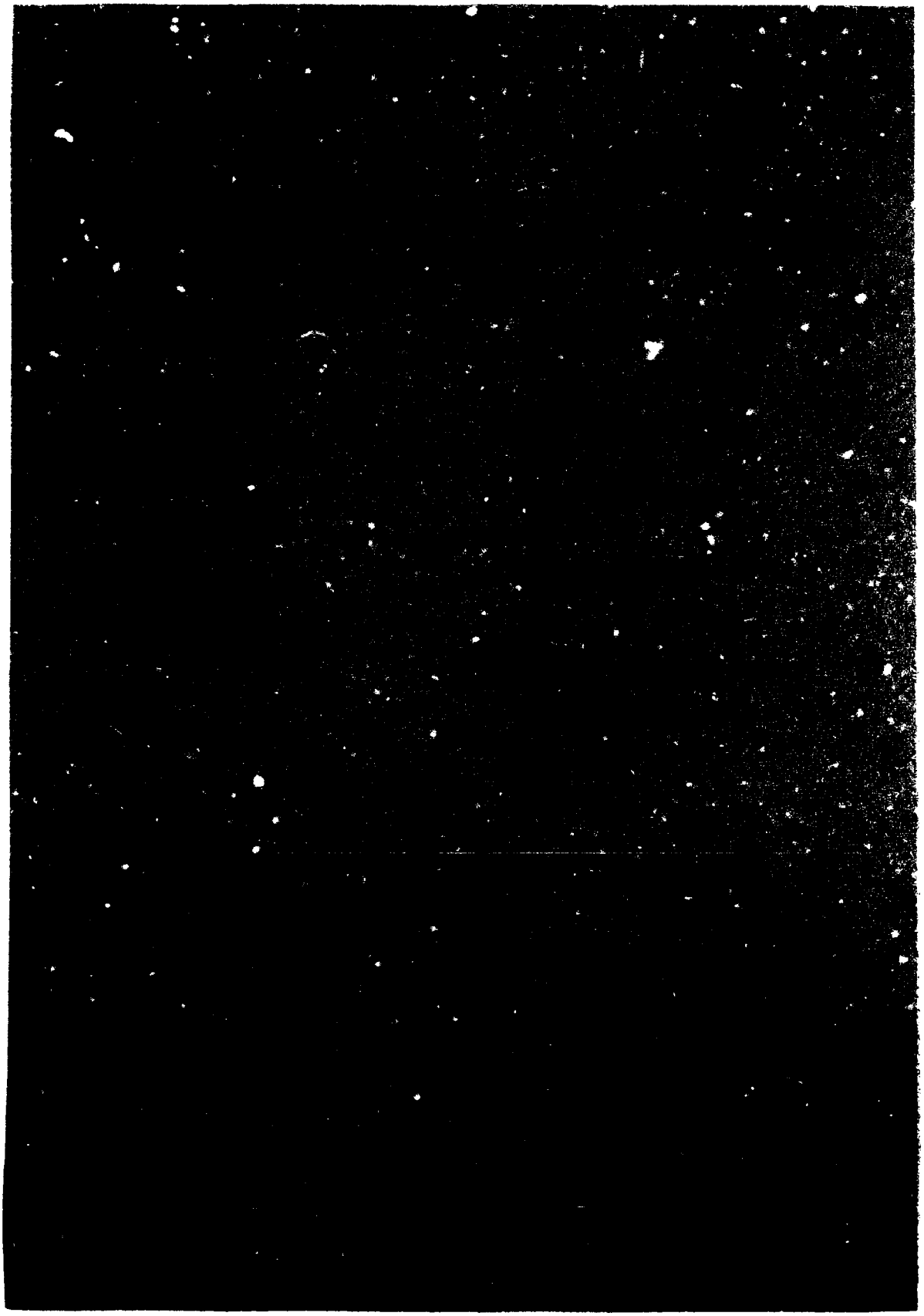

END

DATE
FILMED

8-86